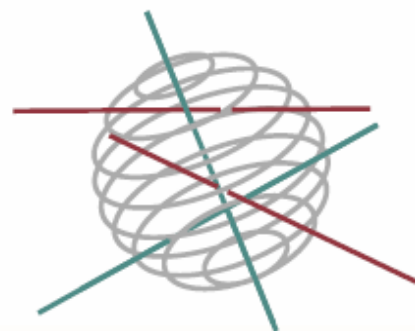


SSD

SCIENCE FOR A SUSTAINABLE DEVELOPMENT

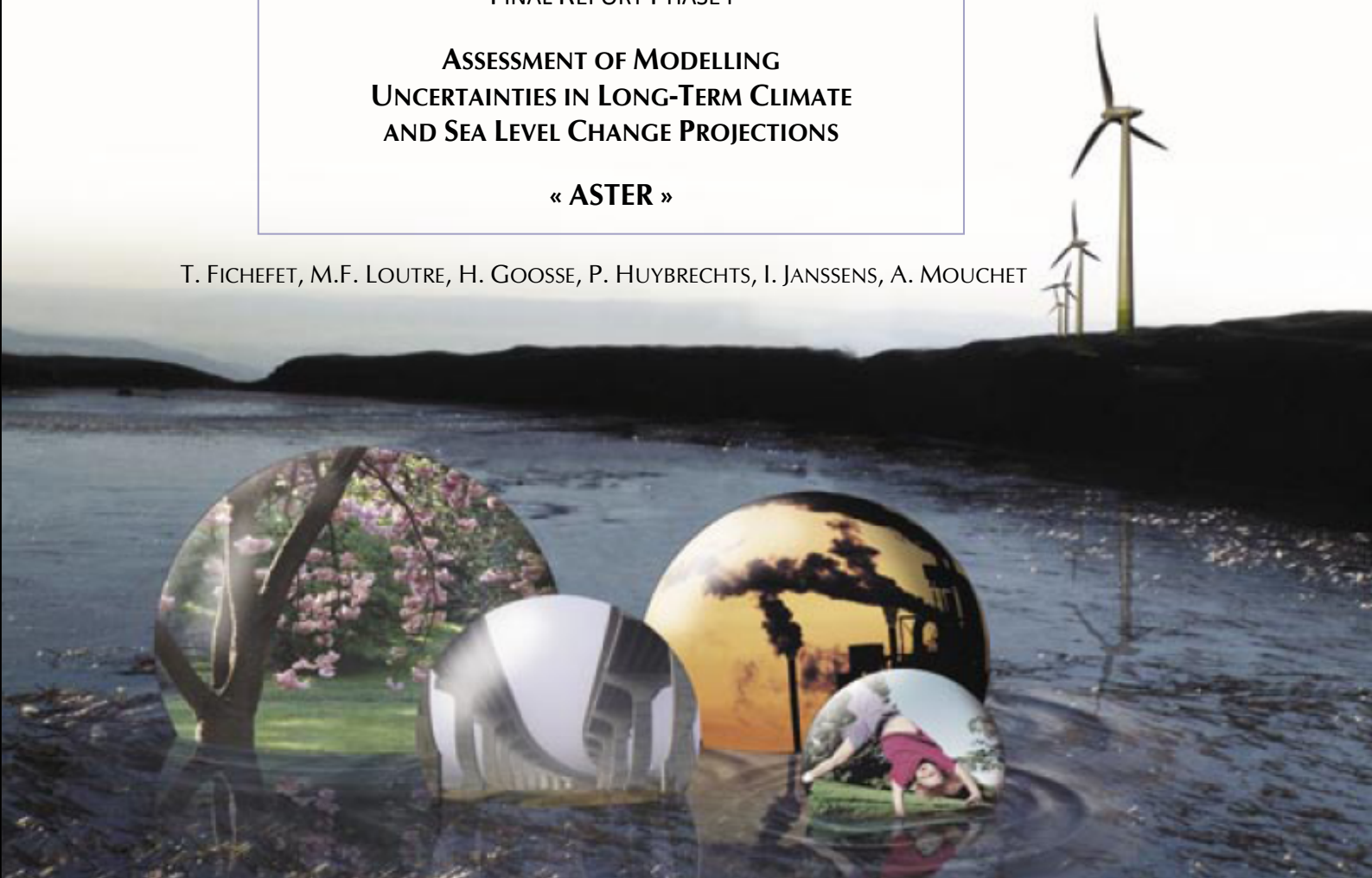


FINAL REPORT PHASE I

**ASSESSMENT OF MODELLING
UNCERTAINTIES IN LONG-TERM CLIMATE
AND SEA LEVEL CHANGE PROJECTIONS**

« ASTER »

T. FICHEFET, M.F. LOUTRE, H. GOOSSE, P. HUYBRECHTS, I. JANSSENS, A. MOUCHET



ENERGY 

TRANSPORT AND MOBILITY 

AGRO-FOOD 

HEALTH AND ENVIRONMENT 

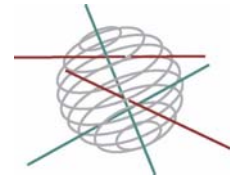
CLIMATE 

BIODIVERSITY   

ATMOSPHERE AND TERRESTRIAL AND MARINE ECOSYSTEMS   

TRANSVERSAL ACTIONS 

SCIENCE FOR A SUSTAINABLE DEVELOPMENT
(SSD)



Climate

FINAL REPORT (Phase I)



**ASSESSMENT OF MODELLING
UNCERTAINTIES IN LONG-TERM CLIMATE
AND SEA LEVEL CHANGE PROJECTIONS
« ASTER »**

SD/CS/01A



Promotors

Thierry Fichefet

Université Catholique de Louvain,
Institut d'Astronomie et de Géophysique
Georges Lemaître (UCL-ASTR)
Chemin du Cyclotron, 2
B-1348 Louvain-la-Neuve

Philippe Huybrechts

Vrije Universiteit Brussel
Departement Geografie (VUB-DGGF)
Pleinlaan, 2
B-1050 Brussels

Anne Mouchet

Université de Liège
Département d'Astrophysique, de Géophysique et d'Océanographie
Laboratoire de Physique Atmosphérique et Planétaire (ULg-LPAP)
Allée du 6 août, 17
Bâtiment B5c
B-4000 Liège



Authors

T. Fichefet, M.F. Loutre, H. Goosse
(UCL-ASTR)

P. Huybrechts, I. Janssens
(VUB-DGGF)

A. Mouchet
(ULg)



BELGIAN SCIENCE POLICY



Rue de la Science 8
Wetenschapsstraat 8
B-1000 Brussels
Belgium
Tel: +32 (0)2 238 34 11 – Fax: +32 (0)2 230 59 12
<http://www.belspo.be>

Contact person: Martine Vanderstraeten
+32 (0)2 238 36 10

Neither the Belgian Science Policy nor any person acting on behalf of the Belgian Science Policy is responsible for the use which might be made of the following information. The authors are responsible for the content.

No part of this publication may be reproduced, stored in a retrieval system, or transmitted in any form or by any means, electronic, mechanical, photocopying, recording, or otherwise, without indicating the reference :

T. Fichet, M.F. Loutre, H. Goosse, P. Huybrechts, I. Janssens, A. Mouchet **Assessment of modelling uncertainties in long-term climate and sea level change projections «ASTER» (SD/CS/01A)**. Brussels : Belgian Science Policy 2009 – 58 p. (Research Programme Science for a Sustainable Development : Final Report Phase 1)

TABLE OF CONTENT

ABSTRACT	4
1. INTRODUCTION	6
2. MODEL DESCRIPTION	9
2.1. AT THE BEGINNING OF THE PROJECT	9
2.2. IMPROVEMENTS	11
<i>Land Bucket Model (LBM)</i>	11
<i>Ocean carbon cycle model (LOCH)</i>	15
<i>Ice sheet model (ISM)</i>	19
3. SELECTION OF THE PARAMETERS	26
3.1. CLIMATE.....	26
3.2. LOCH.....	32
<i>Fertilization effect</i>	32
<i>Vertical flux of POM</i>	34
<i>Rain ratio</i>	35
3.3. CARBON CYCLE AND CLIMATE SENSITIVITY.....	36
<i>2xCO₂ experiments</i>	37
<i>Freshwater hosing experiments</i>	38
3.4. AGISM.....	39
4. EXPERIMENTS	43
4.1. THE LATE HOLOCENE AS A CONSTRAINT FOR THE FUTURE	43
4.2. LAST MILLENNIUM.....	44
4.3. IRREVERSIBILITY OF A MELTING OF THE GREENLAND ICE SHEET IN A WARMING CLIMATE	47
5. CONCLUSIONS AND PERSPECTIVES	49
REFERENCES	50

ABSTRACT

A number of improvements have been made to LOVECLIM, the Earth climate model of intermediate complexity used in the ASTER project. This model consists of five components representing the atmosphere, the ocean and sea ice, the terrestrial biosphere, the oceanic carbon cycle and the Greenland and Antarctic ice sheets. The land surface scheme has been improved to better take into account the impact of the vegetation on the evaporation and bucket depth. The coupling between the ocean-sea ice model and the oceanic carbon cycle model (LOCH) has been revised to guarantee the coherency between the transports of biogeochemical tracers and salinity. The biological module of LOCH has also been adapted. Development work on the ice sheet model has concentrated on additionally incorporating a Northern Hemisphere ice sheet model into LOVECLIM. An important part of the ASTER work was also devoted to the selection of parameter sets that lead to different responses of LOVECLIM to external forcings but still guarantee that the climate simulated for present-day conditions remains close to the observed one. Nine parameter sets were selected, which lead to different climate sensitivities (response to a $2\times\text{CO}_2$) from 1.5°C to 4.0°C and to different reduction of the meridional ocean circulation in response to a freshwater perturbation in the North Atlantic. Similarly, three parameter sets were identified in LOCH that have potentially low, medium and high impacts on the atmospheric CO_2 concentration. Finally, three parameter sets were chosen that control the sensitivity of the ice sheets to warming. The improved version of the climate model together with the selected parameter sets allow evidencing a strong relationship between the simulated decrease in summer sea ice extent in the future and for 8 kyr BP. In other words, if these results are further confirmed, an accurate knowledge of the summer sea ice extent at 8 kyr BP would give a better confidence in the prediction of future evolution of the summer sea ice extent. The possible irreversibility of a disappearance of the Greenland ice sheet in a warming climate was also tested in a series of experiments. According to these experiments, a completely melted away Greenland ice sheet cannot regrow (or very slowly). Only a drastic reduction in atmospheric CO_2 concentration is able to interrupt the melting process but, even in that case, the ice sheet does not regrow. The climate of the last millennium was also simulated with nine 'climatic' parameter sets. The modeled global climatic features are in relatively good agreement with observations. A more detailed analysis of the model results at the regional scale must still be performed. Those experiments lead to reasonable estimates of the carbon fluxes between reservoirs. At this stage, the available datasets do not allow clearly identifying some climate parameter sets as more or less appropriate than others. Several sets yield however major changes in the carbon response when the model is perturbed by a

freshwater flux in the North Atlantic. The ventilation rate of the deep ocean seems to be determinant in setting the atmospheric CO₂ levels in the various sensitivity experiments that were performed.

1. INTRODUCTION

Policymakers are facing a wide range of possible scenarios for long term climate and sea level evolutions without knowing precisely why they differ and how reliable they are. Two factors explain this wide state of affairs: uncertainties in the future anthropogenic emissions of greenhouse gases and aerosols, and uncertainties in the understanding and modeling of the processes that influence the climate.

In particular, the response of the global carbon cycle to human activities is not well constrained and the future levels of atmospheric CO₂ concentrations, for given anthropogenic emissions, are still a major cause of uncertainty. Different coupled Earth system models result in very different predictions of the role of the continental biosphere in driving the atmospheric CO₂ amount at the century time scale, the feedbacks ranging from very positive to negative (e.g., Cox et al., 2000; Friedlingstein et al., 2001; Thompson et al., 2004). On the ocean side, modeling and process studies suggest that an enhanced stratification, a reduced oceanic meridional overturning circulation (MOC) and changes in biology are expected to reduce the solubility and biological CO₂ pumps within one or several centuries (e.g., Maier-Reimer et al., 1996; Sarmiento, 1998; Joos et al., 1999; Schmittner, 2005). Furthermore, recent studies bring concern about the effect of acidification on marine ecosystems (Zondervan et al., 2001; Orr et al., 2005), a fact whose consequences are not known yet. On the one hand, the effect could be a slight increase in ocean CO₂ uptake (Zondervan et al., 2001; Heinze, 2004), but as CaCO₃ shells seem to be very efficient in transferring organic carbon to the deep ocean (e.g. Klaas and Archer, 2002), the longer term effect could be very different.

For a sustained regional, annual mean warming of more than 3°C, the Greenland ice sheet would eventually completely melt away (Gregory et al., 2004). For warmings larger than 10°C, total disintegration could take as little as 1000 years, in which case it would add an average of 7 mm per year to sea level over the period, with wide ranging implications for climate and mankind. The collapse of the West Antarctic ice sheet is considered very unlikely in the next few centuries (Vaughan and Spouge, 2002), but its longer term response remains highly uncertain. The importance of fast response mechanisms, such as ice dynamical changes, still remains to be established (they may be noise on decadal time scales), but if such events would become more widespread and scale with future warming, they would imply greater ice sheet sensitivity to warming than previously considered.

The projected changes in heat fluxes and precipitation over the North Atlantic area as well as interactions with the melting Greenland ice sheet might largely affect the North Atlantic deep water formation and thus the stability of the MOC, with a large potential impact on the climate evolution in the North Atlantic sector and in Europe

(Fichefet et al., 2003). Unfortunately, the magnitude of the MOC response to heat and freshwater perturbations is not very robust among existing models (e.g., Gregory et al., 2005).

Under these circumstances, it is difficult to know which decision should be taken to avoid the most dramatic effects of climate change. However, decisions should be taken in a very near future because one could possibly pass some threshold that would lead to irreversible changes. Because of its large impact on sea level and possibly on the MOC, a particularly important issue of large political significance is whether the ice loss would be reversible or whether there exists a point-of-no-return beyond which the ice sheet disintegration would continue, even if the climate would revert to present conditions.

The general purpose of the study is to provide some guidelines on the range of future climate changes and on the causes of the differences between the various projections. In particular, we focus on the stability of the North Atlantic MOC, on the stability of Greenland and Antarctic ice sheets, on biogeochemical feedbacks and on the impact of all these processes on climate (especially in the North Atlantic, European and polar regions) and sea level. Therefore, we use a coupled Earth system model of intermediate complexity, so that the interactions between the various components of the system can be accounted for. Before studying the future climate, we quantify the ability of our model to reproduce the past. Indeed, future climate scenarios should be checked against the capability of reproducing the past evolution of climate. We focus on the ability of the model to simulate the climate, sea level and atmospheric CO₂ concentration variability and changes.

Different methods have been used to assess uncertainties in modeling past and future climate changes. The most straightforward one is to compare the results from different models under similar conditions. This approach is applied in international model intercomparison exercises such as the Paleoclimate Modeling Intercomparison Project (PMIP) (e.g., Braconnot et al., 2002), the Coupled Model Intercomparison Project (CMIP) (e.g., Covey et al., 2000) or the Ocean Carbon Intercomparison Project (OCMIP) (e.g., Dutay et al., 2004). It was also employed in the previous assessment reports of the Intergovernmental Panel on Climate Change (IPCC) (e.g., Houghton et al., 2001) to document the range of climate model responses to a given scenario of greenhouse gas concentrations. Nevertheless, this method has two important drawbacks. First, major differences in model conception make it difficult to point at a precise cause for different behaviors. Second, it is not possible to sample all the potential range of responses since, in general, only the standard model configurations are utilized in these studies.

In order to explore in a more systematic way the range of possibilities for future climate evolution, it has been proposed to perform large ensemble of experiments in

which some key model parameters are varied within a reasonable range (Murphy et al., 2004; Stainforth et al., 2005). This allows estimating a probability density function of some important climate characteristics like the climate sensitivity (usually defined as the annual mean of the globally averaged surface temperature change resulting from a doubling of the atmospheric CO₂ concentration) or the spatial distribution of the temperature and precipitation changes in response to an increase in greenhouse gas concentrations.

These former studies were conducted with atmospheric general circulation model coupled to models of the oceanic mixed layer and were limited to the study of the equilibrium response of climate to a doubling of the atmospheric CO₂ concentration. Here, we focus on the millennial time scale and employ the fully coupled Earth system model of intermediate complexity LOVECLIM. Compared to coupled general circulation models (CGCMs), LOVECLIM has the advantage of greatly reduced computer requirements, so that a larger number of sensitivity experiments or climate change and sea level scenarios can be conducted. LOVECLIM is therefore an invaluable tool to explore uncertainties in long term climate and sea level change projections. First, some components of the model are improved (section 2). Then some key parameters of LOVECLIM are varied and parameter sets are selected that are leading to very different climate, sea level and atmospheric CO₂ concentration responses to changes in forcing (section 3). Eventually, experiments are performed using the improved version of LOVECLIM and several parameter sets (section 4). They illustrate how some insight can be gained onto the future extent of sea ice (section 4.1). The climate simulated over the last millennium with the selected parameter sets is presented in section 4.2 We study the fate of the Greenland ice sheet over the next centuries under several greenhouse gas forcings in section 4.3. The interaction between climate and carbon cycle is analyzed in section 3.3.

2. MODEL DESCRIPTION

2.1. At the beginning of the project

LOVECLIM-1.0 consists of five components representing the atmosphere (ECBilt), the ocean and sea ice (CLIO), the terrestrial biosphere (VECODE), the oceanic carbon cycle (LOCH) and the Greenland and Antarctic ice sheets (AGISM). ECBilt is a quasi-geostrophic atmospheric model with 3 levels and a T21 horizontal resolution (Opsteegh et al., 1998). It includes simple parameterizations of the diabatic heating processes and an explicit representation of the hydrological cycle. Cloud over is prescribed according to present-day climatology. CLIO is a primitive equation, free surface ocean general circulation model coupled to a thermodynamic-dynamic sea ice model (Goosse and Fichefet, 1999). Its horizontal resolution is $3^{\circ} \times 3^{\circ}$, and there are 20 levels in the ocean. VECODE is a reduced-form model of vegetation dynamics and of the terrestrial carbon cycle (Brovkin et al., 2002). It simulates the dynamics of two plant functional types (trees and grassland) at the same resolution as that of ECBilt. ECBilt-CLIO-VECODE has been utilized in a large number of climate studies (please refer to <http://www.knmi.nl/onderzk/CKO/ecbilt-paper.html> for a full list of references). Interestingly enough, model intercomparison exercises have revealed that the response of the MOC in ECBilt-CLIO-VECODE to changes in greenhouse gas concentrations and to freshwater perturbations is close to the average one of current CGCMs (Gregory et al., 2005; Stouffer et al., 2006). The LOCH model is an oceanic carbon cycle model (Mouchet and François, 1996) that includes an atmospheric module to represent the evolution of CO_2 , $^{13}\text{CO}_2$, $^{14}\text{CO}_2$ in the atmosphere. LOCH is fully coupled to CLIO and runs with the same time step and on the same grid. It takes into account both the solubility and biological pumps. The quantities exchanged are absolute values. LOCH is forced by oceanic temperatures, salinities and velocities, downsloping currents, the horizontal and vertical turbulent diffusivities, the sea ice cover, surface wind speeds and atmospheric pressures. VECODE provides LOCH with the zonally integrated air-biomass carbon fluxes. Combining the carbon fluxes from vegetation and ocean, LOCH computes an annual mean, globally averaged atmospheric CO_2 concentration. Finally, AGISM is composed of a three-dimensional thermo mechanical model of the ice sheet flow, a visco-elastic bedrock model and a model of the mass balance at the ice atmosphere and ice ocean interfaces (Huybrechts, 2002). For both ice sheets, calculations are made on a $10 \text{ km} \times 10 \text{ km}$ resolution grid with 31 sigma levels.

The atmospheric variables needed as an input for AGISM are surface temperature and precipitation. Because the details of the Greenland and Antarctica surface climate are not well captured on the ECBilt coarse grid, these boundary conditions

consist of present-day observations as represented on the much finer AGISM grid onto which climate change anomalies from ECBilt are superimposed. Monthly temperature differences and annual precipitation ratios, computed against a reference climate corresponding to the period 1970-2000 A.D., are interpolated from the ECBilt grid onto the AGISM grid and added to and multiplied by the observed surface temperatures and precipitation rates, respectively. The oceanic heat flux at the base of Antarctic ice shelves is also calculated in perturbation mode using the parameterization proposed by Beckmann and Goosse (2003). After performing mass balance and ice dynamic computations, AGISM transmits the calculated changes in land fraction covered by ice and orography to ECBilt and VECODE. In addition, AGISM provides CLIO with the geographical distribution of the annual mean surface freshwater flux resulting from ice sheet runoff, iceberg calving, runoff from ice free land and basal ice melting. All of these sources of fresh water are added to the surface layer of coastal oceanic grid boxes. Some adjustments are regionally applied to the heat and freshwater fluxes to ensure conservation in the coupled system (see Driesschaert (2005) for details). The Greenland (Antarctic) ice sheet model was first integrated over the last two (four) glacial cycles up to 1500 A.D. with forcing from ice cores to derive the initial conditions for coupling with the other components of LOVECLIM-1.0.

LOVECLIM was utilized to study the evolution of climate, sea level and atmospheric CO₂ concentration over the last few centuries in response to natural and anthropogenic forcings (Fichefet et al., 2007) as well as over the third millennium (Driesschaert et al., 2007). Besides, ECBILT-CLIO, which is the core of LOVECLIM, was employed to investigate, among others, (1) the decadal-to-centennial climate variability in polar regions, (2) the climate dynamics during the Holocene and the Last Glacial Maximum, (3) the abrupt climate change that occurred around 8.2 kyr before present, (4) the evolution of climate over the last millennium, and (5) the predictability of abrupt climate change in a warming climate. It is also worth stressing that LOCH is among those ocean carbon cycle models that are used in the evaluation of inverse techniques designed to estimate anthropogenic ocean carbon invasion using observations as well as in the study of the impact of future anthropogenic CO₂ emissions on ocean biochemistry. Finally, note that AGISM played a central role for dating and interpreting the EPICA (*European project for ice coring in Antarctica*) ice cores.

2.2. Improvements

Land Bucket Model (LBM)

The land surface scheme has been improved in order to better represent the impact of vegetation in the frame of a climate change. It has been modified to take into account the impact of vegetation on evaporation (transpiration) and on the bucket depth (i.e. the maximum water that can be hold in the soil). The variable bucket depth shows a direct implication on the runoff. This has been implemented and tested in LOVECLIM. The goal of the new parameterization is to get a better representation of the feedbacks between vegetation and climate through improvement of the hydrological coupling between them.

Several sensitivity experiments were performed to test the parameterization of the evapo-transpiration flux from the surface ($E + E_{tr}$). So far, evaporation in LOVECLIM was given by:

$$E = \frac{\rho_a}{r_a} \Delta Q \frac{b_m}{b_{\max}}$$

where the aerodynamic resistance r_a depends on the surface drag coefficient and on the wind speed ; ρ_a is the air density; ΔQ is the difference of humidity between the surface and the air layer above ; b_m is the water storage in the soil, and b_{\max} is the bucket depth (the maximum possible value of b_m). The reference value of b_{\max} is 0.15 m (bm15). In sensitivity experiments, it is replaced by either 0.10 m (bm10) or 0.20 m (bm20). A smaller value leads to a decrease in the annual mean precipitation over North America and Europe. The evaporation is therefore reduced together with the latent heat flux. Consequently, the annual mean surface temperature increases in these regions (Figure 1). This feedback is especially active during summer. The combined changes in precipitation, soil water availability and surface temperature yield an increase in grass fraction at the expense of the tree fraction. The broad feature is opposite in case of a larger bucket depth. As far as North Africa is concerned, a reduced value leads to an increase in the desert extent since the soil water content is reduced there. The albedo change induces a cooling in this region. The desert fraction over Sahara is larger for a larger value of this parameter since b_m / b_{\max} decreases in this dry region. The desert increase induces a cooling in winter through the albedo increase, and the decrease in evaporation implies a warming in summer. Those preliminary experiments show that the vegetation is sensitive to the bucket depth.

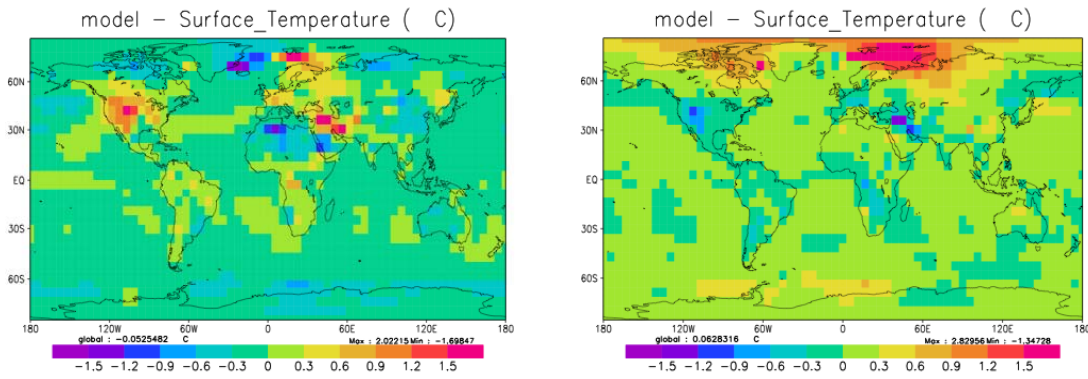


Figure 1 : Annual mean surface temperature (°C). Deviation from the reference simulation (bm15) of (left) bm10 and (right) bm20.

In order to improve the coupling between climate and vegetation, the bucket depth has been made a function of the vegetation and a canopy resistance term has been added. Several parameterizations with increased level of complexity were tested before reaching satisfying results. Only the final formulation of evapo-transpiration is presented here. For this experiment, and in agreement with Milly and Shmakin (2002), the transpiration is given by the following formula and should be later added to the evaporation:

$$E_{tr} = \frac{\rho_a}{(r_a + r_s)} \Delta Q \frac{b_m}{b_{max}}$$

r_s is the canopy resistance and is computed as in SECHIBA (Ducoudré, 1993). The canopy resistance includes both bulk stomatal and leaf aerodynamic resistance. It depends on incident solar radiation (R_s) and on the water vapor deficit of the air (δc) simulated above the canopy, and is inversely proportional to the single sided leaf area index (LAI):

$$r_s = \frac{1}{LAI} \bullet \frac{R_s + R_{s0}}{R_s} \bullet \frac{a + \lambda \delta c}{k_0}$$

The LAI of tree and grass is assumed to vary linearly according to the surface temperature (T_s): $LAI = LAI_{max} (0.2 + 0.04 \times T_s)$, LAI_{max} being 6 for trees and 2 for grass.

The parameters are as follows:

R_{s0}	125 W m ⁻²
a	23×10 ⁻³ kg m ⁻³
λ	1.5
k_0 (grass)	30×10 ⁻⁵ kg m ⁻² s ⁻¹
k_0 (tree)	25×10 ⁻⁵ kg m ⁻² s ⁻¹

b_{\max} is a weighted average for the whole grid area. It will be hereafter referred to as $b_{\max_ave} \cdot b_{\max}$ for desert is 0.05 m, 0.15 m for grass and 0.3 m for forest. The transpiration term is now computed separately for each vegetation type of a given grid cell in order to explicitly take into consideration that the area fraction covered by desert has a shallower rooting depth than the area covered by forest or desert. Therefore, it is corrected in the following way:

$$E_{bare} = \frac{\rho_a}{r_a} \cdot \Delta Q \cdot \frac{b_m}{b_{\max_ave}} \cdot \frac{b_{\max_des}}{b_{\max_tree}}$$

$$E_{tr_grass} = \frac{\rho_a}{r_a + r_s} \cdot \Delta Q \cdot \frac{b_m}{b_{\max_ave}} \cdot \frac{b_{\max_grass}}{b_{\max_tree}}$$

$$E_{tr_tree} = \frac{\rho_a}{r_a + r_s} \cdot \Delta Q \cdot \frac{b_m}{b_{\max_ave}}$$

Evapo-transpiration is then computed as the sum of evaporation (E) and transpiration (E_{tr}):

$$E + E_{tr} = 1 \cdot E_{bare} + F_{grass} \cdot E_{tr_grass} + F_{tree} \cdot E_{tr_tree}$$

where F is the fraction of the grid cell covered either by grass or trees.

The experiment testing this parameterization (lbn5) shows as broad feature a strengthening of forests and deserts (Figure 2). There is a cooling over North Western America, Western Europe and South of Africa. This cooling is related to an increase in latent heat flux since the concerned regions are forested areas. There is a warming in the northern part of Africa for the opposite reason. There is also a strong warming over the entire Arctic region, which is due to the increase in tree fraction at high northern latitudes decreasing the albedo there in autumn and winter. The impact on vegetation is an increase in the forest extent over Western Europe and most of North America at the expense of grass. The desert extends over most of Northern Africa and also over Eastern Europe.

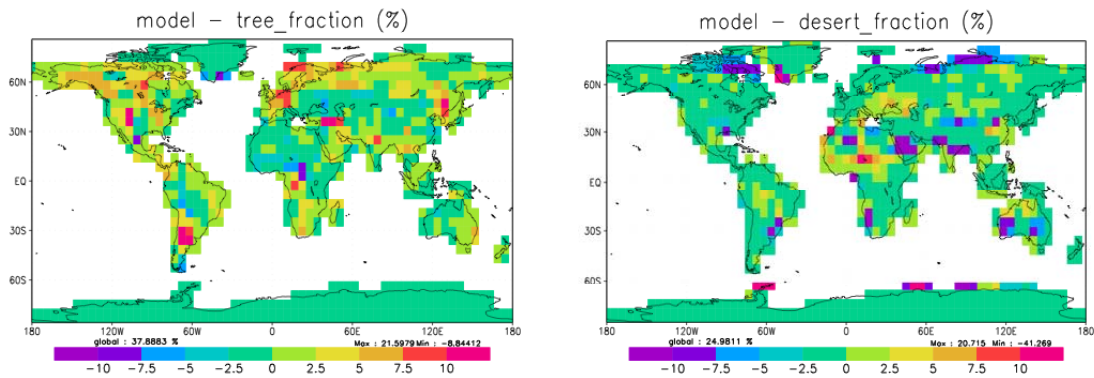


Figure 2 : Vegetation change (in lbm5) either forest (left) or desert (right) compared to the reference simulation.

The lbm5 parameterization was kept in LOVECLIM because it exhibits a reasonable response. It is worth mentioning that the feedbacks between vegetation and climate related to climate change between the Holocene and the present-day are enhanced. However, further detailed sensitivity experiments should be performed to confirm that result. Some bias of the model could not be solved by the improvement performed because they result from an unrealistic pattern of precipitation in LOVECLIM (e.g. wrong location of desert in South America and Africa).

The stability of LOVECLIM, including this new surface scheme, has then been tested. Two long equilibrium simulations (2000 yr) were performed, i.e. the Holocene (some 6000 years ago) and preindustrial climates. In both cases, it was checked that the global annual mean surface temperature, the globally averaged ocean temperature and the intensity of the meridional overturning circulation do not exhibit any long term drift. The preindustrial climate is characterized by an annual global mean surface temperature of 16.1°C, i.e. 0.3°C higher than with the former land surface scheme. The hydrological cycle is also slightly amplified on a global scale (increase in precipitation and evapo-transpiration). Table 1 below provides other characteristic values of the simulations.

On an annual average, the surface temperature is too warm (compared to data) over the tropical regions (between 30°N and 30°S) and up to 60° in the Southern Hemisphere (Figure 3). However, polar regions (Arctic and Antarctic) are cooler than observations. The simulated annual mean precipitation is in good agreement with observations pole ward of 30°. However, the model cannot reproduce the large precipitation rates observed in the equatorial regions and overestimates precipitation in the tropical regions (Figure 3). The model simulates more forested area over most of the continents, except for the Eurasian boreal forest, which is underestimated compared to observations. However, it has to be mentioned that our preindustrial simulation does not take into account the human deforestation, which is present in the observations. The deforestation is estimated to be 30% on a global scale. This

improves considerably the agreement between model and observations. Desert fraction is underestimated over Sahara and Arabia. The Chile desert and the African forest are not well located.

	Preindustrial	Holocene
Ts (°C)	16.1	16.4
pp (cm/yr)	107.05	108.32
SST (°C)	19.0	19.1
To (°C)	3.23	3.34
NH sea ice area – Max (km ²)	~14×10 ⁶	~14×10 ⁶
NH sea ice are – min (km ²)	~7×10 ⁶	~5×10 ⁶
MOC (in the North) (Sv)	~28	~28

Table 1 : Some global features of the simulated climate for the preindustrial and the Holocene (6kyr BP) periods. Ts (surface temperature), pp (precipitation), SST (sea surface temperature), To (global mean ocean temperature), MOC (maximum of the meridional streamfunction).

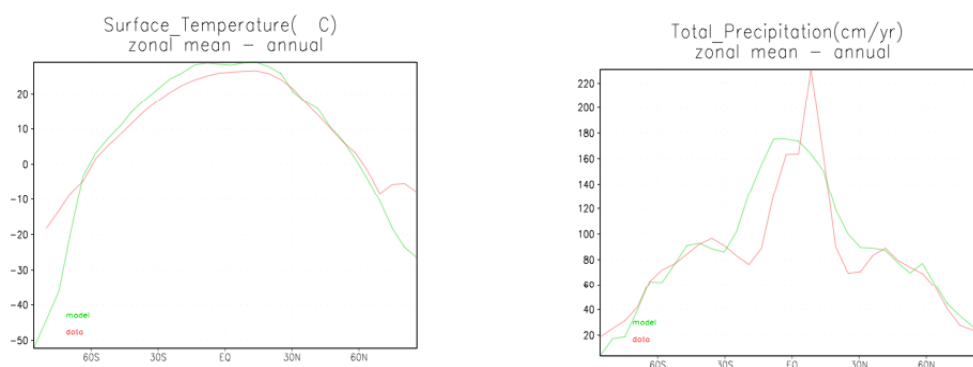


Figure 3 : Zonal distribution of the simulated annual mean surface temperature (left) and annual precipitation (right) for the preindustrial forcings.

The major feature of the mid Holocene climate is a greening of the Sahara desert. The Holocene simulation shows indeed a decreased fraction of desert and an increased fraction of grassland over the Sahara region compared to the preindustrial values. There is also an increase in the tree fraction over the Sahel region at 6kyr BP compared to the preindustrial period. This vegetation change is associated with a large precipitation increase over Sahara, as well as over Arabia.

Ocean carbon cycle model (LOCH)

The interface coupling LOCH to CLIO was built in order to guarantee that the transports of tracer and salinity are coherent. However, the vertical advection scheme used in CLIO is a 2nd order centered scheme. In order to compute the isotopic ratios and to avoid negative concentrations, it would be an advantage to be able to use a scheme that guarantees monotonicity. A hybrid vertical advection scheme was implemented in LOCH. This scheme was tested off-line and leads to reasonable results. However, when applied in the on-line version, the uptake of

anthropogenic CO₂ was much too large (exp. 1hg-1 in Figure 4 and Table 2). After analysis, it became clear that a numerical noise linked to the inertial term in CLIO caused the vertical velocity in the deep ocean to oscillate with significant amplitude at a high frequency. This translated into a large numerical diffusivity with the hybrid vertical scheme, which resulted in too much mixing of tracers between the surface and the deep ocean. This numerical noise diminished drastically when computing the Coriolis term in the equation of motion in a totally implicit way in replacement of the former semi-implicit scheme. This modification yields a dramatic decrease in the anthropogenic CO₂ ocean uptake (exp. stdAM-1 in Figure 4 and Table 2).

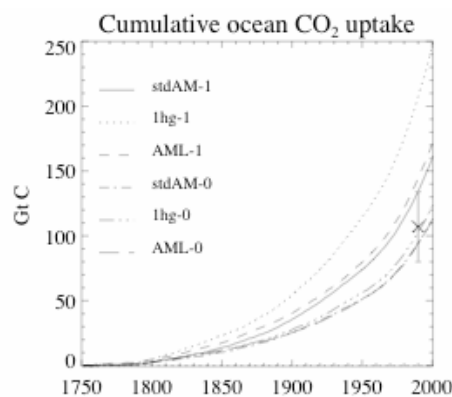


Figure 4 : Effect of the implicit factor in the Coriolis term on ocean anthropogenic CO₂ uptake. This factor is 1. for experiment stdAM, 0.75 for exp. AML and 0.5 for exp. 1hg. Two different schemes for the vertical transport of tracers were used: a 2nd order centered scheme (exp. “-0”) and the hybrid 1st order scheme (exp. “-1”). The vertical bar represents the data-based estimated ocean uptake of anthropogenic CO₂ (Houghton, 2001).

An important change dealt with relaxing the requirement of total mass balance. In the former LOCH version, rivers automatically compensated for any matter loss to the sediments. In a similar way, evaporation/precipitation imbalances were corrected. The updated version allows the user to choose between, on the one hand, automatically adjusting fluxes and, on the other hand, prescribed (non-balancing) external fluxes. The differences in the outcome of the model are negligible when considering the industrial era and the coming centuries. However, on much longer time scales, this decoupling may be of importance, especially when addressing circulation or biogeochemical changes.

Experiment	Vertical scheme	Implicit factor Coriolis term	Air sea CO ₂ flux during the 80's (PgC/yr)	Air sea CO ₂ flux during the 90's (PgC/yr)
1hg-1	hybrid	0.50	3.20	3.93
1hg-0	centered	0.50	1.66	1.99
AML-1	hybrid	0.75	2.33	2.66
AML-0	centered	0.75	1.59	1.80
stdAM-1	hybrid	1.00	2.06	2.54
stdAM-0	centered	1.00	1.51	1.78
OCMIP-2			1.56--2.42	1.80--2.80
IPCC TAR			1.3--2.5	

Table 2 : This table lists the ocean uptakes of CO₂ during the 80's and 90's (rows 4 and 5 respectively) for sensitivity experiments to the numerical schemes. The transport scheme is given in column 2, while column 3 contains the implicit factor for the Coriolis term. The last two lines show estimates from the OCMIP-2 models and from IPCC TAR.

Major adaptations of LOCH are related to the biological module. Silica has the potential to play a significant role in the ocean biochemistry at the long time scales. In climate change experiments performed with LOVECLIM1.0, the main perturbation of the ocean biology was a decrease in silica in the surface ocean at high latitudes (Fichefet et al., 2007). In that version, dissolution of opal is solely allowed in the deepest level (S1 hereafter). We tested other dissolution schemes : one in which opal shells are homogeneously distributed in the water column (S2), then a 3d scheme (S3) with temperature dependent rate and depth control (Bidle et al., 2002; Fuji and Chai, 2005). When examining the global model behavior (Figure 5), the scheme with bottom dissolution seems to perform slightly better at reproducing the ocean dissolved silica distribution. However, the global opal export rate increases from 75.4 Tmol/yr in S1 to 91.4 Tmol/yr in S3 (field estimates point toward a value less or equal to 120 Tmol/yr (Nelson et al., 1995)). The fraction of the export production supported by diatoms in the model also increases from 38% in S1 to 46% in S3. The latter value is very close to the commonly accepted 50% figure (Nelson et al., 1995). The difference between schemes 1 and 3 is that the second allows a refueling of the euphotic layer consistent with the seasonal time scale. These schemes were also tested with a circulation representing differently the ocean water masses (experiments "A" in Figure 5). The same conclusions may be drawn.

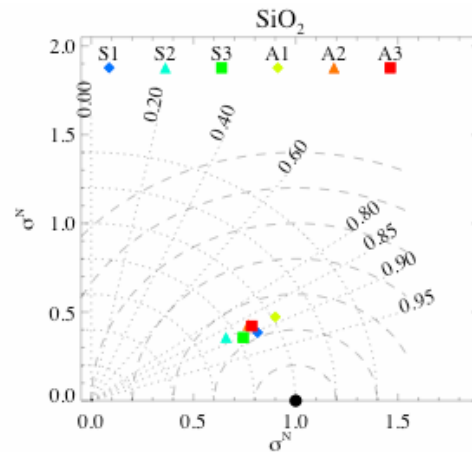


Figure 5 : Taylor diagram for the experiments with different silica dissolution schemes. The reference (climatological field (Boyer et al., 2006)) is represented by the filled circle on the abscissa. Each experiment corresponds to a different symbol, which is displayed on the top of the figure for reference. Results correspond to the LOVECLIM circulation (label starting with an “S”) or to another circulation (“A”). The numbers refer to the dissolution scheme: 1 (bottom), 2 (homogeneous) and 3 (temperature). The radial distance from the origin is proportional to the standard deviation of the pattern (σ^N) normalized to that of the data. The centered RMS difference between the test and reference field is proportional to their distance apart. The correlation coefficient between the two fields is given by the cosine of the angle between the abscissa and the line joining the origin to the symbol corresponding to the test field (Taylor, 2002).

The biological module in LOCH is based on the computation of the export production (that is the net carbon flux out of the euphotic zone). This export production is determined in a non linear way from the availability of nutrients and the growth of a primary producer pool. In the standard LOCH version, this biomass pool is considered as being a standing stock, resulting in a tight link between nutrients and export. We adapted the biomass pool so that it is now fully submitted to the 3D transport. Further developments of the biological module were carried out in collaboration with the ISMAL team. This new version considers three phytoplankton groups (diatoms, photosynthetic cyanobacteria and other phytoplankton species), each group being characterized by its own growth and grazing rates. Nitrogen was also added to the model; its cycle includes N_2 fixation and denitrification. This model version has been successfully tested with the annual mean circulation fields and is currently being tested with the seasonal circulation. The significance of all these modifications is currently being assessed. This version is not part of LOVECLIM1.1. However, this doesn't exclude any further studies with improved biogeochemical cycles. In that respect, it is worth mentioning that, in parallel to the ASTER project, LOCH is being implemented in the 3D circulation model of the Mediterranean Sea in collaboration with the GHER group and the ISMAL team. This collaboration offers a unique opportunity to validate LOCH over an area where the characteristic temporal and spatial scales are shorter and where more data are available.

MEDUSA (Munhoven, 2007) is a transient one-dimensional advection–diffusion–reaction model describing the coupled early diagenesis processes of carbonates, organic matter and opal in the surface sediment. A new extended version has been made available to the project. MEDUSA now also includes equations for the ^{13}C isotopic signature of the considered carbon bearing components (calcite, aragonite, organic matter, CO_2 , HCO_3^- , and CO_3^{2-}).

MEDUSA has been successfully tested in two different setups:

- . in offline mode with boundary condition datasets generated by LOCH, in the same configuration as the one used with LOVECLIM;
- . in asynchronous coupled mode with the LOCH version that uses the LSG grid. Steady state simulations as well as glacial-interglacial simulations (120 kyr) were performed.

Some residual problems, typically related to the remineralization of the organic matter, still need to be solved. The coupling between LOCH and MEDUSA is now completed. The version of LOCH compatible with MEDUSA is totally similar to the LOCH version imbedded in LOVECLIM; this was achieved through the development of a « black box » sediment model.

Ice sheet model (ISM)

Most of the ice sheet model development work has concentrated on incorporating the Northern Hemisphere ice sheet model (NHISM; Zweck and Huybrechts, 2005) into LOVECLIM. NHISM is a three-dimensional thermo-mechanical ice sheet model, which includes an improved scheme for marine calving to better simulate ice sheet expansion and contraction over shallow marine basins such as the Arctic Ocean shelf. The model is implemented on a 50 km horizontal resolution, larger than the coarse T21 resolution of ECBilt to sufficiently capture the details of the topography and the width of the ablation zone around the margin. The NHISM resolution, on the other hand, is still coarser than the 10 km resolution of AGISM (Antarctic and Greenland Ice Sheet Models). That is because of the larger model domain and because boundary conditions can be less well specified during glacial times than for the present-day ice sheets. Furthermore, the higher resolution of AGISM is required to better represent the marginal outlet glaciers that are mostly topography controlled. The apparent discrepancy between the numerical resolution of the ice sheet and atmospheric components are not at odds with each other as climatic changes tend to vary on much larger spatial scales than, e.g., bedrock topography.

The scheme of the coupling between NHISM and LOVECLIM is depicted in Figure 6 (left panel). The coupling is fully interactive and two-way between the ice sheets, at the one hand, and the ocean and atmosphere at the other hand. Procedures similar

to those employed previously for the coupling of AGISM with ECBilt and CLIO were adopted. The AGISM and ECBilt-CLIO-VECODE exchange information once a year. The seasonal cycle of surface temperature, computed by the atmospheric model, is also transmitted to AGISM. Surface temperature and precipitation changes are considered in perturbation mode. Corrections are applied to close the freshwater and heat balances. AGISM computes the land fraction covered by snow and ice over Greenland and the topography of each ice sheet, and transmits them to ECBilt. Each AGISM grid cell is associated with a single ECBilt grid cell, over which the value of the variable is computed by averaging or summing. AGISM also provides CLIO with the freshwater flux (directly or indirectly) from the ice sheets. The continental runoff model (CRM) determines for every land point the discharge pathway that water will follow to reach the ocean and attributes the runoff to the corresponding CLIO oceanic cell. Temperature and precipitation modeled by ECBilt are transmitted to AGISM as difference (for temperature) and ratio (for precipitation). Moreover, the values are interpolated onto the AGISM grid through a Lagrangian interpolation. CLIO provides an estimate of the heat flux at the base of the Antarctic ice shelves.

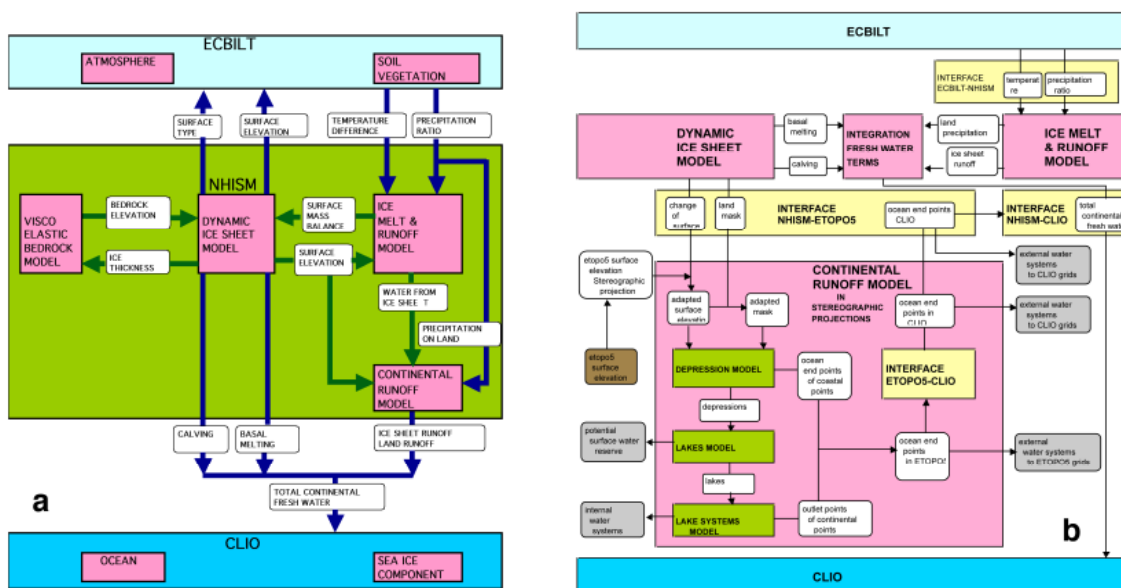


Figure 6 : Scheme of the coupling procedure between NHISM and LOVECLIM. (a): general procedures; (b): details of the continental runoff model (CRM).

The key parameters needed as input for NHISM are the surface temperature and the precipitation rate. At this stage, climatic changes provided by ECBILT are downscaled in the perturbation mode by superimposing temperature anomalies and precipitation ratios (climate changes versus control) from the T21 atmospheric grid onto the 50 km grid of NHISM. This procedure is implemented because the climatic patterns produced by ECBILT differ from observations. Temperature perturbations are applied monthly, but precipitation ratios are imposed annually. Further tests are

however needed to investigate whether the precipitation rate from ECBILT could be applied directly; this procedure should provide a better representation of the orographic forcing over the former ice sheets. The interpolation of data from the coarse atmospheric grid relies on interpolation with Lagrange polynomials. Conversely, ECBILT takes into account changes in surface type and surface elevation caused by the evolution of ice sheets on the continents of the Northern Hemisphere.

For the coupling between NHISM and CLIO, the procedure is more complicated. The ice sheets provide freshwater fluxes from iceberg calving and melt water runoff, and, to a minor extent, from basal melting. As long as the ice sheet borders the coastline or is near to it, it can be readily assumed that the freshwater flux will enter the nearest grid cell of CLIO, and a simple allocation scheme suffices. However, most margins of the Northern Hemisphere ice sheets in North America and Eurasia are located far away from the ocean. The produced melt water therefore needs to be routed through the existing lake and river system. Since the evolution of the ice sheets entails large modifications of the surface orography, both from the weight of the ice mass and from isostatic uplift after retreat, large temporal changes in the runoff routing are expected (e.g. Tarasov and Peltier, 2005). Moreover, the ice sheets are known to be able to create ice-dammed lakes during their retreat, and the associated freshwater release may follow unexpected pathways, including under the ice sheets themselves.

We therefore developed a novel hydrological melt water routing scheme that takes into account a variable surface relief and is able to determine the discharge pathway that the surface water will follow from any continental location to the coast. These can then be grouped together for any bordering CLIO grid cell. The allocation is unique. A basic assumption is that the melt water does not evaporate en route, nor infiltrates into the soil. It is furthermore assumed by the scheme that any depression will entirely fill before spilling over at its lowest margin. Time dependent issues related to reservoir filling and emptying are neglected assuming that the freshwater fluxes are large compared to any lake water storage changes (which is equivalent to assuming a steady state).

Crucial input to the melt water routing scheme is a high resolution representation of the surface topography. We used the ETOPO5 (1988) dataset on 5 x 5 minutes of arc resolution. This corresponds to a resolution of about 9.25 km of latitude and 4.6 km of longitude at 60°N. Although this resolution is still rather coarse to properly resolve all of the narrower valleys, an alternative is not readily available. In recent years, ETOPO5 has been superseded by ETOPO2 (2' resolution) and GTOPO30 (30" resolution), but the latter datasets only show the continental surface and have not been merged with the oceanic bathymetry. They also do not show the bottom

topography of the Great Lakes, as does the ETOPO5 dataset. That seriously limits their application in a crucial area of lake formation during ice sheet retreat. The higher resolution datasets would also put too high demands on computer memory and run times.

The continental runoff scheme in NHISM is implemented through the following steps:

1. *Setup of the interpolation procedure of the NHISM (50 km resolution) onto the ETOPO5 grid.* This is required because changes in NHISM topography are applied to the ETOPO5 topography in anomaly mode to account for the evolving surface. Use is made of Lagrange polynomials of an order to be selected in the code. The work is performed on a transformed representation of the ETOPO5 data on a 6.25 km x 6.25 km grid for the same stereographic projection as employed in NHISM (called ETOPO5SP). In this way, every 8th grid point in ETOPO5SP coincides with a NHISM grid point.

2. *Inventory of coastal areas and continental depressions.* A mask is first constructed to distinguish between continental and oceanic grid points relative to a variable sea level. Using surface gradients, an endpoint is tracked for every ETOPO5SP grid point. An endpoint is the lowest continental surface topography or the first oceanic point that can be reached. If the endpoint borders the ocean, the ETOPO5SP grid point belongs to a coastal area. Otherwise, when the endpoint is on land, the continental grid point belongs to a continental depression. The possibility exists to use another contour than sea level to construct the continental mask. Depressions are furthermore defined as consisting of sets of points with the same endpoint. Flat areas are sometimes characterized by a long series of very small depressions.

3. *Grouping of depressions into lakes.* An algorithm is applied to locate adjacent depressions and to find out whether they have a common overflow point, i.e. whether they would merge into a larger lake when filled with water. The procedure is repeated for adjacent depressions until the total number of lakes formed in this way no longer decreases. Convergence is usually reached after applying the search algorithm for about 20 times. The result consists of large depressions or (potential) lakes together with their drainage area.

4. *Documentation of the lakes.* A record is made of the area and volume of the lakes, together with the area of the drainage basin and the coordinates and elevation of the outlet (overflow point). The possibility exists to incorporate evaporation as a control on the lake level, but for now, the scheme assumes that, at all times, sufficient water is available to fill all depressions.

5. *Grouping of lakes into internal drainage systems.* For all lakes, it is determined into which lower lake it will overflow, i.e. into which contiguous depression having a lower outlet. The process is repeated until the ocean is reached. In this way, all lakes can

be grouped for the same 'endlake', i.e. the last lake before the ocean is reached. This defines an internal drainage basin having the same outlet into the ocean, i.e. the outlet of the endlake.

6. *Construction of external drainage systems.* It is now possible to link any continental point to a specific point bordering the ocean (ocean point), be it directly for a point belonging to a coastal area or indirectly for a point belonging to a continental depression. The result is a series of external drainage systems grouping all points draining into the ocean through the same ocean point. Many external drainage systems arise in this way of largely varying size, some of which consist of only one ETOPO5 grid point.

7. *Allocation of any ocean point to a CLIO grid cell.* A search algorithm is applied to group all ocean points draining into the same CLIO grid cell. The procedure is based on the nearest neighbor principle as the CLIO coastline does not exactly coincide with the coastline generated in the ETOPO5SP dataset. In this way, any continental ETOPO5 grid point is linked to a specific CLIO grid cell.

8. *Allocation of NHISM grid points to a CLIO grid cell.* For every NHISM 50 km grid point, it is determined what is the corresponding collection of ETOPO5SP grid points where ice sheet runoff is released. In this way, any NHISM grid point not by itself bordering the ocean where calving can take place is linked to a specific CLIO grid cell. The scheme is therefore able to partition runoff in the right proportion into respective CLIO cells.

The above procedure is schematically depicted in Figure 6 (right panel). The hydrological routing scheme can also be used to establish the discharge pathway of continental precipitation. In that case, however, an additional treatment of evaporation is required to conserve the total water fluxes over the continents. An additional complication is the treatment of endoreic regions of interior drainage such as the intermountain southwest of the United States and the arid zones in central Asia. In the hydrological model, such basins will entirely fill before spilling over at their lowest exit. This does not affect ice sheet runoff in North America. However, it means that e.g. ice sheet runoff destined for the Caspian Sea will ultimately end up in the Mediterranean via the Black Sea and the Bosphorus.

In LOVECLIM, there is no coupling between changes in the ocean and NHISM, which interaction in the full model is only implemented for the Antarctic component (AISM).

A direct product of the hydrological routing scheme is the delineation of drainage basins. The model determines for every individual continental location the discharge pathway that surface water will follow to reach the ocean. These pathways can then be grouped together to delineate contiguous drainage basins, which drain into the

same oceanic grid cell. During the simulations, the procedure needs to be regularly updated to take into account changes in surface topography caused by ice sheet evolution. This is effectuated every 100 years. Figure 7 shows an example of the delineation over the Northern Hemisphere continents. Some artifacts still remain. These can mostly be explained by the resolution of ETOPO5SP and the slight smoothing produced by the initial map projection transformation. In cases where a major river cuts through a narrow valley, this may cause artificial lakes, which may ultimately drain into another catchment area and CLIO grid cell.

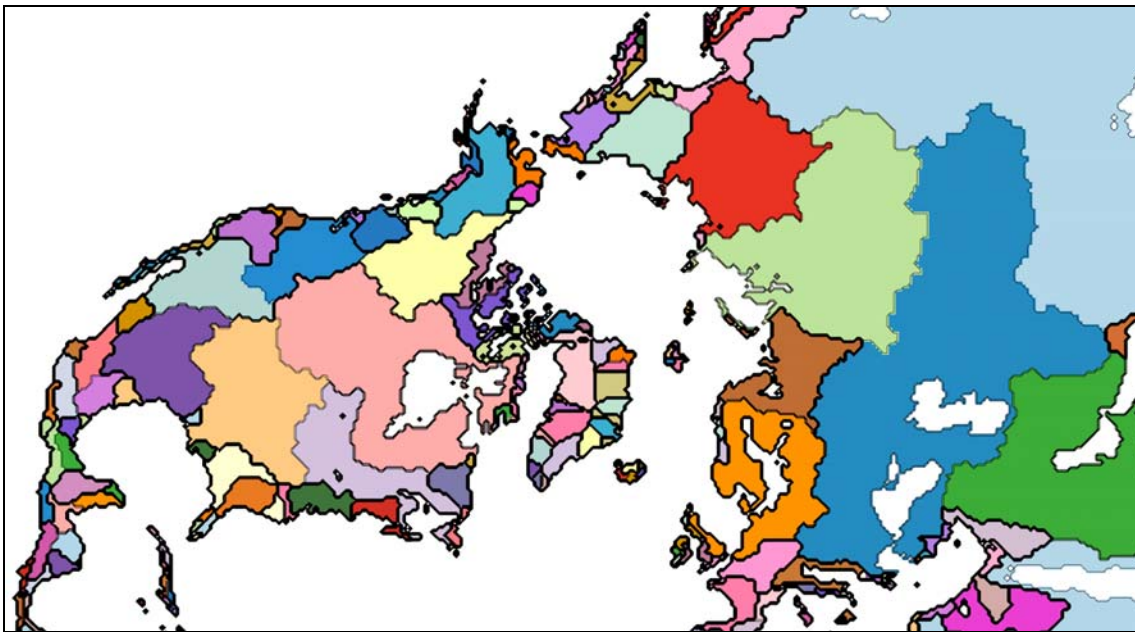


Figure 7 : The continental runoff model (CRM) determines for every land point the discharge pathway that surface water will follow to reach the ocean. Each color represents an area, which drains into the same CLIO oceanic cell. Large catchment's areas in central Asia with no apparent outlet are in fact bordering the NHISM grid; drainage resulting from such areas is grouped together and spread out evenly over the global ocean.

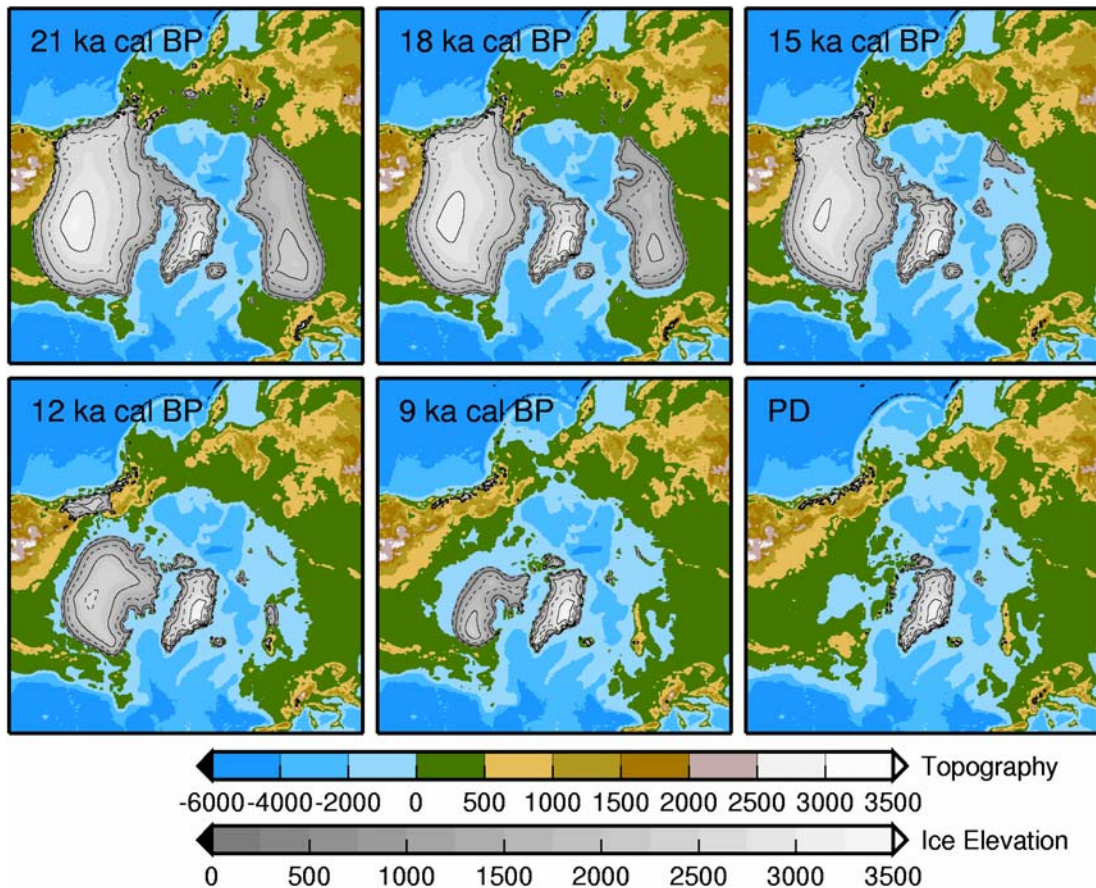


Figure 8 : Results from a preliminary offline simulation of the Northern Hemisphere ice sheets with NHISM forced by ECBILT-CLIO at an asynchronous time step of 200 years.

First testing of the interfaces between NHISM, at the one hand, and ECBILT and CLIO, at the other hand, gave satisfactory results. However, the hydrological routing model in CRM requires some further refinements to better represent runoff from continental areas below current sea level and from continental shelves that may become exposed during periods of lower sea level, such as the Hudson Bay and the Barents Sea. Since the ASTER experiments only deal with the last part of the last glacial-interglacial transition, initial conditions are required for 10,000 years BP. These will be taken from a precursor experiment in which NHISM has been coupled with ECBilt-CLIO in asynchronous mode for the period since the Last Glacial Maximum (Figure 8). In this experiment the ice sheet input into ECBilt was prescribed from a gridded representation of ice sheet extent together with a simple parabolic profile to obtain ice sheet elevation at a 200-year resolution. The present-day land-ocean mask was kept constant and feedback between the ice sheets and the global ocean was switched off. To avoid unwanted model drift in the Holocene simulations with LOVECLIM, it may be required to spin the coupled model up from an earlier starting date in synchronous mode, e.g. from 15,000 years ago. Further testing is planned for the near future to properly decide which avenues are best to take here.

3. SELECTION OF THE PARAMETERS

3.1. Climate

We selected model parameter sets that produce reasonable simulations of the present-day climate and that lead to contrasted simulated responses to a doubling of the atmospheric CO₂ concentration and to a freshwater hosing. Therefore, we identified several sets of parameter values chosen within the range of validity of those parameters (Table 3).

Name (1)	<i>I</i> 2 (2)	<i>L</i> 4 (2)	<i>amplw</i> (3)	<i>explw</i> (3)	<i>albocef</i> (4)	<i>albice</i> (5)	<i>avkb</i> (6)	<i>CorA</i> (7)
E11	0.125	0.070	1.00	0.3333	1.000	0	1.0 (8)	-0.0850
E21	0.125	0.070	1.00	0.4	0.900	0	1.5	-0.0850
E31	0.131	0.071	1.00	0.5	0.950	0	2.5	-0.0850
E41	0.131	0.071	1.10	0.5	0.900	0	2.5	-0.0850
E51	0.131	0.071	1.30	0.5	1.050	0.02	2.0	-0.0850
E12	0.120	0.067	1.00	0.4	0.900	0	2.0	0.0000
E22	0.125	0.070	1.00	0.4	0.900	0	1.5	-0.0425
E32	0.125	0.070	1.05	0.5	0.900	0	1.5	-0.0425
E52	0.125	0.070	1.30	0.5	1.000	0.02	1.5	-0.0425

Table 3 : The nine climatic parameter sets selected for ASTER.

(1) The name of the experiments has been designed to provide a quick overview of their main characteristics:

The first digit is related to the quasi-equilibrium response of the model to a doubling of the CO₂ concentration in the atmosphere, as obtained in a 1000 year experiment in coupled mode:

- 1 corresponds to a climate sensitivity lower than 2.0°C;
- 2 corresponds to a climate sensitivity between 2.0 and 2.5°C;
- 3 corresponds to a climate sensitivity between 2.5 and 3.0°C;
- 4 corresponds to a climate sensitivity between 3.0 and 3.5°C;
- 5 corresponds to a climate sensitivity between 3.5 and 4.0°C.

The second digit is related to the response of the model to a freshwater dumping in the North Atlantic, which linearly increases at a rate of 0.1 Sv per 500 years (reaching thus a flux of 0.2 Sv after 1000 years):

- 1 corresponds to a decrease of **less** than 50% of the maximum of the MOC after 1000 yr;

2 corresponds to a decrease of **more** than 50% of the maximum of the MOC after 1000 yr.

The third and fourth digits will be related to the response to the ice sheet and of the carbon cycle to a perturbation, respectively

(2) I_2 and I_4 are two parameters used in the Rayleigh damping term of the equation of the quasi-geostrophic potential vorticity. I_2 corresponds to the 500-800 hPa layer of the model, while I_4 corresponds to the 200-500 hPa layer (see equation 1 of Opsteegh et al. (1998) and equation 11 of Haarsma et al. (1996)).

(3) The simple long wave radiative scheme of LOVECLIM is based on an approach termed the "Green's function method" (Chou and Neelin, 1996; Schaeffer et al., 1998). The scheme could be briefly represented for clear sky conditions by the following formula for all the model levels:

$$Flw = Fref + FG(T, GHG') + G1 * amplw * (q')^{**} explw$$

where Flw is the long wave flux, $Fref$ is a reference value of the flux when temperature, humidity and the concentration of greenhouse gases are equal to the reference values, FG is a function, not explicitly described here, allowing to compute the contribution associated with the anomalies compared to this reference in the vertical profile of temperature (T) and in the concentration of the various greenhouse gases in the atmosphere (GHG'). The last term represents the anomaly in the long wave flux due to the anomaly in humidity q' . The coefficients $Fref$, $G1$ and those included in the function FG are spatially dependent. All the terms have been calibrated to follow as closely as possible a complex general circulation model long wave radiation scheme (Schaeffer et al., 1998), but large uncertainties are of course related to this parameterization, in particular as the model only computes one mean relative humidity between the surface and 500 hPa, the atmosphere above 500 hPa being supposed to be completely dry.

(4) The albedo of the ocean in LOVECLIM depends on the season and location. At each time step, it is multiplied by $albcoef$ in the experiments analyzed here. For a typical albedo of the ocean of 0.06, using a value of 1.05 for $albcoef$ increases the value of the albedo to 0.063.

(5) The albedo of sea ice is based on the scheme of Shine and Henderson-Sellers (1985), which uses different values for the albedo of snow, melting snow, bare ice and melting ice. For thin ice, the albedo is also dependent of the ice thickness. If $albice$ is different from zero in the experiments discussed here, the value of the albedo in the model is increased by $albice$ for all the snow and ice types.

(6) As explained in detail in Goosse et al. (1999), the minimum vertical diffusivity in the ocean follows a vertical profile similar to the one proposed by Bryan and Lewis (1979). The coefficient $avkb$ is a scaling factor that multiplies the minimum values of the vertical diffusivity at all depths. A value of $avkb$ of 1 (1.5, 2, 2.5) corresponds to a minimum background vertical diffusivity in the thermocline of 10^{-5} m²/s (1.5×10^{-5} , 2.0×10^{-5} , 2.5×10^{-5} m²/s).

(7) As ECBILT systematically overestimates precipitation over the Atlantic and Arctic Oceans, it has been necessary to artificially reduce it over the Atlantic and Arctic basins (defined here as the oceanic area north of 68°N). The corresponding water is dumped into the Pacific Ocean, a ocean over which the model precipitation is too weak (Goosse et al., 2001). $CorA$ corresponds to the percentage of reduction of the precipitation in the Atlantic.

(8) In LOVECLIM1.1, the Coriolis term in the equation of motion is computed in a totally implicit way because the semi-implicit scheme used for this term in LOVECLIM1.0 (Driesschaert et al., 2007) induced too much numerical noise. The older scheme has been kept here in experiment E11 only, in order to have an easier comparison with the results of LOVECLIM1.0. Because of the larger implicit diffusion associated with this scheme, a lower value of the explicit diffusion is applied in E11.

For each set, three experiments are carried out. A control run under preindustrial conditions is first performed until equilibrium. This simulation is conducted to check that the present-day climate for each selected parameter set is in relatively good agreement with observations. The equilibrium state is then used as initial state for the next two experiments. First, a simulation is conducted in which the atmospheric CO₂ concentration increases by 1% per year during 70 years from the preindustrial value (277.5 ppm) until twice the present-day value (555 ppm). The run is then continued with this constant value until equilibrium (Figure 9, left). Second, an experiment in which the amount of freshwater added in the North Atlantic (30-60°N) linearly increases by 0.1 Sv in 500 yr (i.e. a rate of 0.0002 Sv/yr) (Figure 9, right). Two main indices are selected to characterize the response of the model to the prescribed perturbations, i.e. the increase in global annual mean surface temperature after 1000 years in the doubling CO₂ experiment from the equilibrium value and the percentage of decrease in the MOC after 1000 years in the water hosing experiment. Although not exactly the same as the model used in Driesschaert et al. (2007), model E11 is sharing many climatic features with this nominal model. Its sensitivity is rather low (1.6°C for the 2×CO₂ simulation and a 20% reduction of MOC after 1000 years for the water hosing experiment). In a first step, we used LOVECLIM without interactive ice sheets and carbon cycle. We identified 9 model parameter sets, which sensitivity to a doubling of the atmospheric CO₂ concentration ranges from 2 to 4°C (Table 4).

Figure 10 shows that the phase space (temperature, MOC) is rather homogeneously covered. The names of the experiments (Table 4) have been designed to provide a quick overview of their main features. The first digit is related to the quasi-equilibrium response of the model to a CO₂ doubling and the second digit is related to the response of the model to freshwater dumping in the North Atlantic (1 (resp. 2) corresponds to a decrease of **less** (resp. **more**) than 50% of the maximum of the MOC after 1000 yr). In this case, number one corresponds to the parameters used in the nominal version of the model. The third and fourth digits are related to the response to the ice sheet and of the carbon cycle to a perturbation, respectively. Here, a number two corresponds to the parameters used in the nominal version of the model. An experiment with only two digits stands actually for an experiment with nominal values for the ice sheet and carbon cycle. In other words, 22 should be added to the experiment name.

It must also be underlined that the model parameter sets simulate different equilibrium states with respect to the MOC (Table 4). Moreover, the time decrease in the meridional overturning function (in the water hosing experiment) shows several features according to the model parameter sets (Figure 11, right). Indeed, for some model parameter sets (e.g. E11), the MOC decreases almost linearly, while others (e.g. E12) display a more abrupt reduction of the circulation. This should be kept in mind for the interpretation of future simulations.

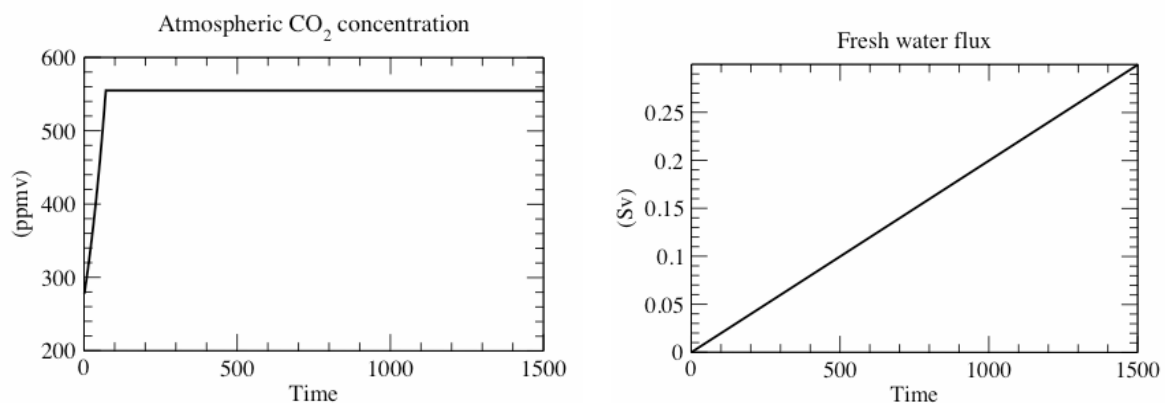


Figure 9 : Scenario for the perturbation scenarios. Left: atmospheric CO₂ concentration ; right: freshwater dumping in the North Atlantic.

	Climate sensitivity (1) (°C)	MOC sensitivity (2) (%)	Equilibrium MOC (3) (Sv)
E11	1,6	-16	28,2
E21	2,1	-28	25,9
E31	2,6	-20	25,2
E41	3,2	-16	24,7
E51	3,9	-34	23,5
E12	1,8	-52	17,5
E22	2,1	-57	23,3
E32	2,7	-54	20,5
E52	3,6	-51	20,0

- (1) the increase in global annual mean surface temperature after 1000 years in the doubling CO₂ experiment from the equilibrium value
- (2) the percentage of decrease in the MOC after 1000 years in the water hosing experiment
- (3) the equilibrium strength of the meridional stream function in the North Atlantic (Sv).

Table 4 : Main features of the model response with respect to climatic parameter sets selected for ASTER.

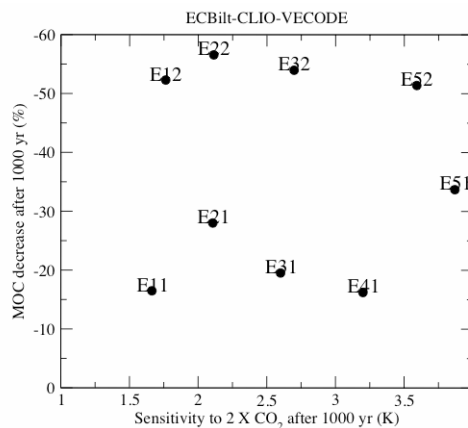


Figure 10 : Distribution of the model parameter sets in the phase space (temperature, MOC).

The same kind of selection of model parameter sets is then extended to the fully coupled LOVECLIM model. In this case, as the AGISM model is running in anomaly mode, the new reference simulated climate state, corresponding to the period 1970-2000 A.D., has been recomputed for each parameter set. The sensitivity experiments start from a quasi-equilibrium state for which all the forcings are kept constant to their preindustrial values during 1500 years of simulation.

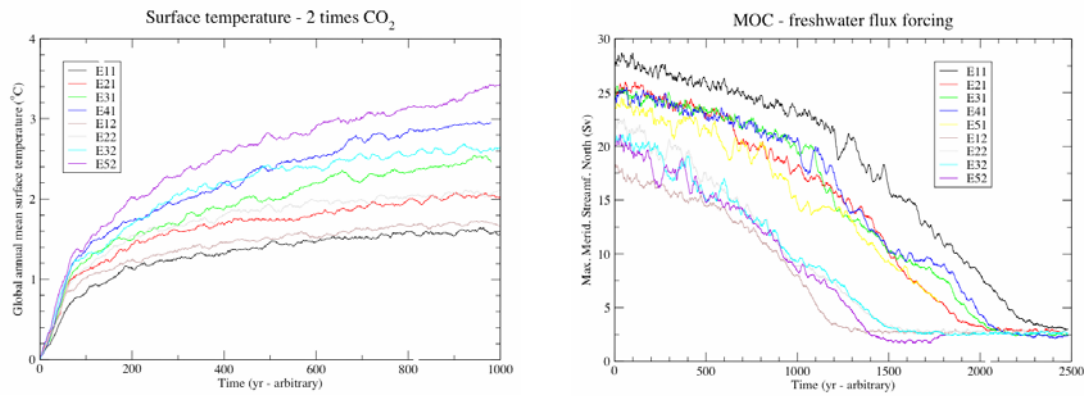


Figure 11 : Time evolution of the model response according to the selected model parameter sets in the perturbation experiments : (left) doubling of the CO₂ concentration and (right) freshwater dumping. Temperature is presented as deviation from the initial value and MOC changes are the actual values.

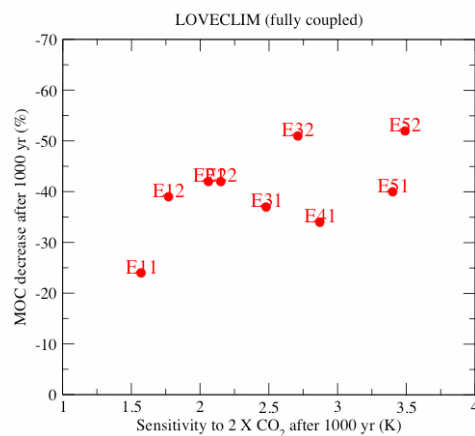


Figure 12 : Distribution of the model parameter sets in the phase space (temperature, MOC) for the LOVECLIM model.

The results of these sensitivity tests, as displayed in the phase diagram (Figure 12) show that the climate sensitivity of the model is not strongly affected by the coupling with the Greenland and Antarctic ice sheets. The range of sensitivity reached by the different parameter sets is similar with or without the coupling, i.e. from 1.6°C to 3.8°C. However, the response of the meridional overturning circulation to a freshwater perturbation is significantly different with and without the coupling with AGISM. More precisely, the presence of the ice sheets seems to play a damping role. Indeed, those parameters sets (experiments Ex1) that induce a weak reduction of the MOC in uncoupled mode display an enhanced response in coupled mode. On the other hand, those parameters sets (experiments Ex2) that induce a strong reduction of the MOC in uncoupled mode exhibit a reduced response in coupled mode. A detailed analysis of this behavior has not yet been completed because, first of all, we want to be sure that it is not an artifact either of the coupling procedure or of the experimental setup of the experiments.

3.2. LOCH

The key parameters for the carbon cycle were chosen among those that have a strong impact on the marine biogeochemical cycle and on the response of atmospheric CO₂ to emission scenario. The sensitivity experiments dealt with the continental vegetation fertilization effect, on the one hand, and the rain ratio and the vertical flux of POM in the ocean, on the other hand. We review these three themes in the following and conclude with the choice of the parameter sets that will be specified for the project experiments.

Fertilization effect

LOVECLIM predicts a larger uptake by the continental biosphere under warmer climate than without (Fichefet et al., 2007). This response contradicts other studies (Friedlingstein et al., 2006). Up to 70% of the response of the vegetation carbon stock in LOVECLIM comes from the fertilization effect, while the climate is responsible for the remaining 30%.

This fertilization effect is parameterized by the following formula :

$npp = npp_0 (1 + \beta \ln(p \text{ CO}_2 / p \text{ CO}_{2ref}))$, where npp is the net primary production, $p \text{ CO}_2$ the CO₂ atmospheric pressure, and npp_0 and $p \text{ CO}_{2ref}$ the npp and $p \text{ CO}_2$ for a reference state, respectively.

The fertilization effect constitutes a negative feedback on CO₂. Under ideal conditions, this effect may be quite large for some ecosystems (e.g. +25% to 60% for young trees under CO₂ doubling; +14% for a mixture of grassland and crops; IPCC TAR). For natural forest ecosystems, the magnitude of the effect is poorly known and might be low or negligible. It appears that limitations including nutrients and water constrain the ecosystem response to CO₂ (Reich et al., 2006; Pitman and Stouffer, 2006). The standard value for β in VECODE is 0.36, which is the npp increases by 25% for CO₂ doubling. As there are different fertilization responses according to the ecosystem, we separated the fertilization effect into two terms: one for grass and one for forests. In addition to the standard case ($\beta = 0.36$), two sets of parameters were determined that lead to a lower fertilization effect.

The impact of a change in the fertilization response may only be assessed in transient simulations with increasing atmospheric CO₂. We therefore performed two transient experiments for each couple of β parameters. A preindustrial equilibrium run was followed by atmospheric forcing:

a CO₂ concentration scenario for which the atmospheric CO₂ increases to 2×CO₂ within 70 years and is maintained at that level afterwards. The run lasted 600 years. In that case, the ocean response is similar for the three fertilization experiments.

a CO₂ emission scenario for which emissions during the industrial era follow reconstructions. From 2000 A.D. emissions keep on increasing up to around 2050 A.D., then stabilize and stop in 2100 A.D.. The experiment was carried out over 1000 years. The ocean uptake varies according to the different fertilization effects.

There were no other radiative forcing than CO₂ and no deforestation. For each scenario a control run of the same duration was performed in parallel. The magnitude of the sensitivity of the model to CO₂ fertilization may be evaluated from Table 5 and Figure 13.

Exp.	β_g	β_t	Atm. CO ₂ (μatm)	
			2100 A.D.	2749 A.D.
VgE1	0.36	0.36	690	453
VgE2	0.50	0.14	716	464
VgE3	0.22	0.14	752	489

Table 5 : Atmospheric CO₂ in 2100 A.D. (column 4) and 2749 A.D. (column 5) as obtained from sensitivity experiments on the vegetation response to CO₂ under the emission scenario. The values of the fertilization factors for grass (β_g) and for trees (β_t) corresponding to each experiment are respectively given in columns two and three

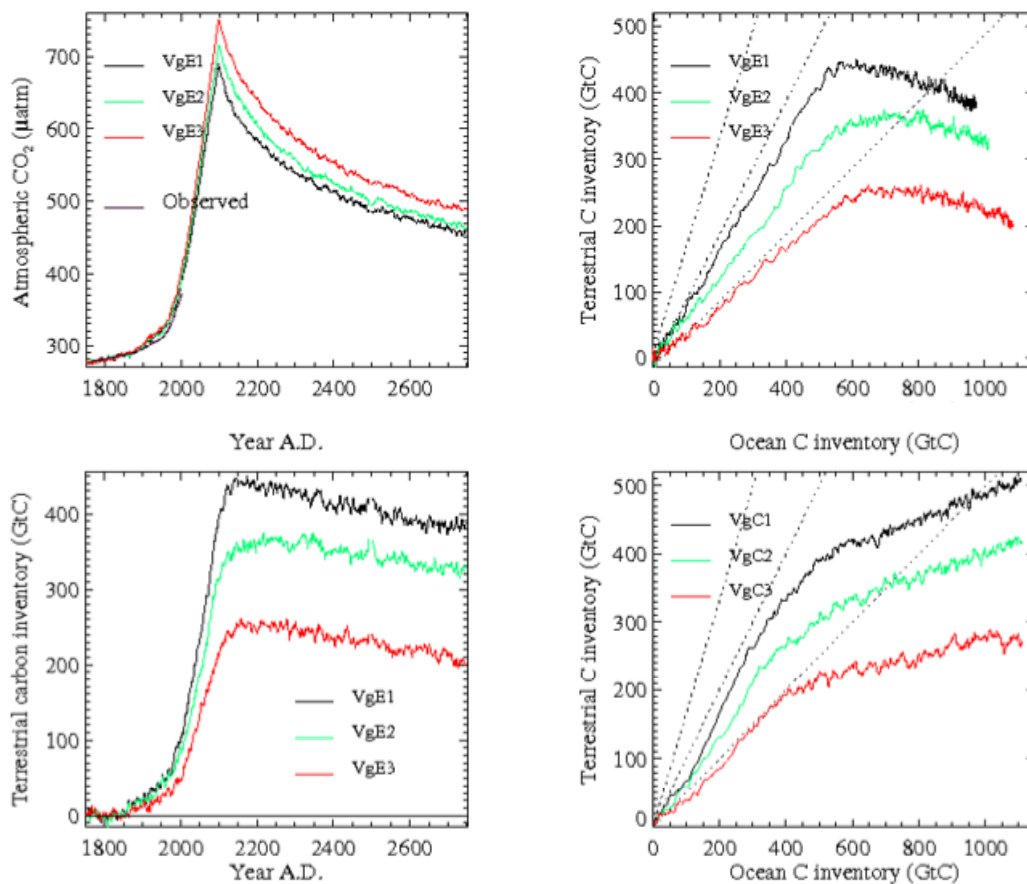


Figure 13 : Temporal evolutions of atmospheric CO₂ and terrestrial carbon stock under the emission scenario (left panels) for the various experiments listed in Table 5. Terrestrial carbon inventory versus ocean carbon inventory for the emission scenario (top right) and for the concentration scenario (bottom right). Lines with slope 2:1, 1:1, and 1:2 (dashed, clockwise) are also shown in these two panels. Inventories are presented as anomalies with respect to the control run.

Vertical flux of POM

The vertical flux of POM is one factor controlling the sequestration of CO₂ in the deep ocean. It is usually represented by a power law z^α , with z being the depth (Martin et al., 1987). A shallow profile leads to a larger export production by making nutrients more readily available in the upper ocean. But this may be accompanied by a less effective carbon sequestration in the deep ocean. Several distributions were proposed (Figure 14), which correspond to different ocean provinces or different estimation methods. We varied the α factor from -0.950 to -0.648 in LOCH and obtained the response summarized in Table 6.

α	-0.950	-0.858	-0.750	-0.500
export pr. (GtC/yr)	6.5	6.2	5.7	5.3

Table 6 : Export production (GtC/yr) obtained with different POM distribution profiles.

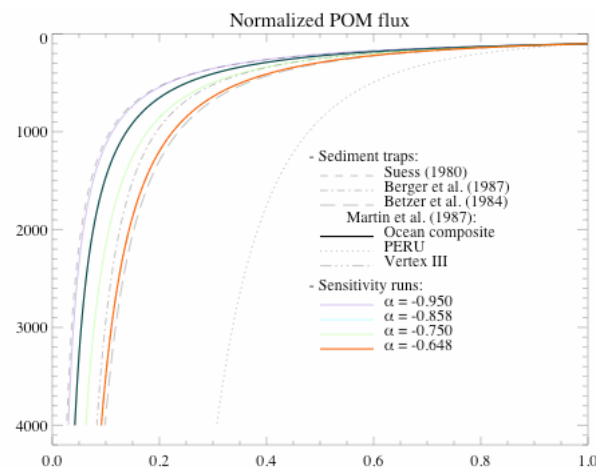


Figure 14 : Evolution of the POM flux with depth as derived from the literature and as simulated by the model. These fluxes have been normalized to their value at 100m. The sensitivity experiments performed with LOCH correspond to the color curves.

Rain ratio

The buildup of calcium carbonate shells in the surface ocean results in a CO₂ source to the atmosphere, while dissolution constitutes a sink. The global value of the calcium carbonate flux to the deep ocean is not well constrained. The rain ratio (the ratio of carbon in shells to that in soft tissues) exhibits a large range of values. The canonical global value of 0.25 has been revised downward as present-day estimates point toward a value around 0.1 (Archer, 2003; Najjar et al., 2007). Smaller values of this rain ratio are observed in more productive areas where diatoms usually dominate the food web (Tsunogai and Noriki, 1991). The rain ratio in LOCH is controlled among other terms by the assimilation of silica. Two sets of parameters were determined. With the first set, a global rain ratio of 0.07 is obtained, with the second a value of 0.12. As LOCH contains a carbonate compensation mechanism, rain ratio changes also impact on the dissolution of calcium carbonate in the deep ocean. With the larger rain ratio, we obtain a downward calcium carbonate flux of 66 Tmol.C/yr and dissolution amounts to 48 Tmol.C/yr. The lower rain ratio results in the precipitation of 38 Tmol.C/yr with the dissolution of most of it (32 Tmol.C/yr).

The different parameters related to the ocean carbon cycle were tested interactively with the climate over the historical period as well as over the next centuries by forcing the model with an anthropogenic emission scenario. The response of the atmospheric CO₂ remained well within that obtained with previous versions of the model. On short time scales, changes in the rain ratio or in the export production have a negligible impact on the atmospheric CO₂. For example, the atmospheric CO₂ partial pressure in 2100 A.D. changes by at most 7 μatm across experiments performed with the different parameters for the rain ratio and the POM flux. This change is within the variability produced by the model and can't be ascertained yet. Table 7 summarizes possible combinations of the parameters in the carbon cycle with possible low to high impacts on atmospheric CO₂.

β _g	0.14	0.14	0.36
β _t	0.22	0.50	0.36
α	-0.848	-0.648	-0.648
Rain ratio	0.07	0.07	0.12

Table 7 : Model parameter sets for the carbon cycle.

3.3. Carbon cycle and climate sensitivity

In this section, we present the results of experiments performed with the full carbon cycle model for the nine climate parameter sets (see section 3.1 for details on these versions). For each of these parameter sets the sensitivity experiments of section 3.1 were repeated without AGISM but with active carbon cycle. For 2xCO₂ experiments, there is no feedback on the climate, since the atmospheric CO₂ is constrained. On the other hand, in freshwater hosing experiments with active carbon cycle, the atmospheric CO₂ is prognostic. Hence, the climate response to the addition of freshwater in the North Atlantic might differ from that presented in section 2.1 since those experiments were performed with a constant atmospheric CO₂ concentration.

For a given climate parameter set an equilibrium run of a duration of 1500 years was performed with the atmospheric CO₂ maintained constant. This equilibrium provides the initial state for the two transient experiments (2xCO₂ and freshwater hosing). Each transient experiment is accompanied by a control run, which may be seen as the continuation of the equilibrium with the difference that atmospheric CO₂ is prognostic in the control run of the freshwater hosing experiment. Another difference arises from relaxing the condition of a strict conservation of tracers whenever dilution or concentration occurs. The two control runs allow evaluating whether the transient experiments results are significant or not in term of carbon exchange between reservoirs.

The model drift in the control experiments is low. Unless stated otherwise, the results presented in this section refer to anomalies that are the difference between the experiment and the corresponding control.

2xCO₂ experiments

The 2xCO₂ forcing does not lead to any significant change in the ocean biogeochemical cycles. Some reorganization occurs as the extent of sea ice decreases with increasing surface temperatures, but changes in global figures remain negligible after 1 kyr.

Ocean CO₂ uptake is inversely correlated with sea surface temperature (SST) hence with model sensitivity (Figure 15- left). Two factors explain the spread of ocean carbon inventories: a lower solubility with increasing temperatures and a lower ventilation rate. Indeed, a climate parameter set leading to a larger sensitivity implies a lower exchange rate between the deep ocean and the surface, hence a lower CO₂ invasion rate.

On the other hand, the land carbon inventory increases with increasing model sensitivity (Figure 15 - middle). The larger temperatures favor the growth of vegetation in formerly non-productive areas. This process is accelerated by the fertilizing effect of CO₂. The role of fertilization is clearly evidenced in the right panel of Figure 15. Without any fertilization effect the terrestrial carbon inventory is about 25% that obtained with fertilization. This result is similar to that obtained with the previous version of LOVECLIM (Fichefet et al., 2007).

The results for experiments E12, E22 and E32 are comprised between those of E11 and E51, and exhibit the same behavior with respect to model sensitivity as the experiments illustrated in Figure 15.

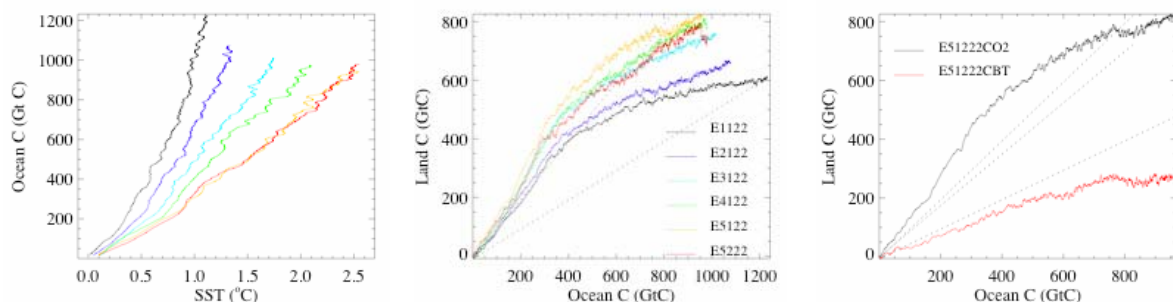


Figure 15: 2x CO₂ experiments: temporal evolutions of ocean carbon inventory versus SST (left) and of terrestrial carbon inventory versus that of ocean (middle). The same colors are used in the left and middle panels to identify experiments. The right panel presents results with (E5122CO2) and without (E5122CBT) considering the CO₂ fertilization effect on the terrestrial biosphere.

Freshwater hosing experiments

In freshwater hosing experiments, the atmospheric CO₂ concentration evolves in response to the carbon uptake or release by the ocean and the terrestrial biosphere. A (moderate) increase in atm CO₂ (less than 15 μatm) occurs with most model versions after 1.5 kyr (Figure 16- left and right panels). The change in atmospheric CO₂ concentration for experiment E52 is much larger, up to 60 μatm. In every experiment, the land releases carbon (Figure 16) at a rate determined by the evolution of surface temperatures. The atmospheric CO₂ level is then determined by the capacity of the ocean to absorb the excess CO₂. The slight decrease in atmospheric CO₂ for E1122 after 1.5 kyr results mostly from the larger ventilation rate associated to that model version with the SST change playing a marginal role.

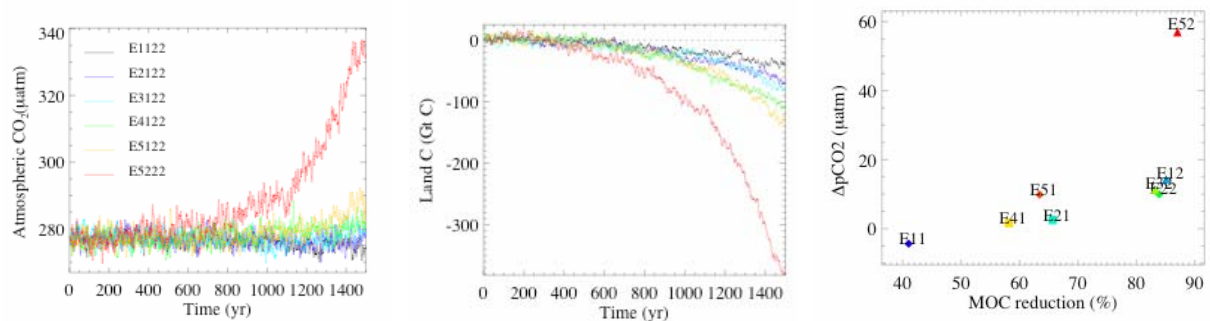


Figure 16: Freshwater hosing experiments: temporal evolutions of atmospheric CO₂ (left) and of terrestrial carbon inventory (middle). The same colors are used in the left and middle panels to identify experiments. The CO₂ levels at the end of the experiment (1.5 kyr) are plotted against the percentages of MOC reduction at the same time in the right panel.

The role of the terrestrial biosphere in the increase in atmospheric CO₂ concentration is highlighted with two additional experiments. We reproduced experiments E1222 and E5222 by imposing that the terrestrial vegetation does not have any impact on the atmospheric CO₂. This was achieved by zeroing the carbon fluxes to and from the continents. As illustrated in Figure 17 the response of the system is drastically different.

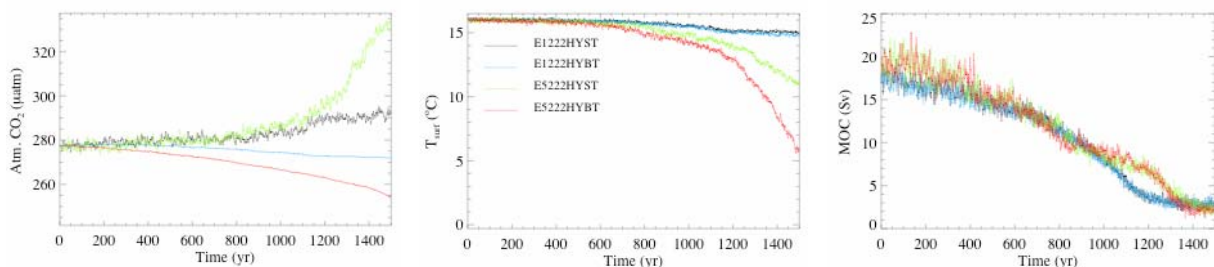


Figure 17: Freshwater hosing experiments: atmospheric CO₂ concentrations (left), mean global surface temperature (middle) and MOC (right) evolutions with time for experiments with full carbon cycle (HYST) and experiments with the sole influence

from the ocean on the carbon cycle (HYBT). The same colors are used in all panels to identify experiments.

Experiments with the modified carbon cycle (E1222HYBT and E5222HYBT) both exhibit a significant decrease in atmospheric CO₂ concentration with respect to their counterpart with the full carbon cycle (E1222HYST and E5222HYST); with the climate parameter set of E52, the difference in atmospheric CO₂ is larger than 75 µatm. The lower CO₂ levels result, through radiative changes, in much lower surface temperatures (Figure 17 - middle). The lower temperatures also lead to a diminution in terrestrial vegetation cover (not illustrated), which constitutes a positive feedback and hence participates to the decrease in surface temperatures.

3.4. AGISM

For the Antarctic and Greenland ice sheets, it was decided to withhold three different parameter sets, which control the ice sheet sensitivity along the ‘melting axis’. These 3 model versions of AGISM are respectively referred to as ‘low’ (index 1 in the experiment name), ‘mid’ (index 2), and ‘high’ (index 3); the ‘mid’ model versions are identical to the standard version of AGISM used so far in LOVECLIM, and which was tuned to best reproduce the current ice sheets and their assumed sensitivity to climate change. Table 8 gives an overview of the parameter set selected to this effect.

Parameter	‘low’ sensitivity	‘mid’ sensitivity standard version	‘high’ sensitivity
AGISM			
Basal melting below ice shelves [m/yr]	Constant at 0.25	According to net heat input below the cavity	Triple the amount of the ‘mid’ run
SIGMA (standard deviation melt model) [°C]	4.0	4.5	5.0
DDFS (positive-degree-day factor for snow melting) [m/yr/PDD]	0.75*0.003	0.003	1.25*0.003
DDFI (positive-degree-day factor for ice melting) [m/yr/PDD]	0.75*0.008	0.008	1.25*0.008
GISM			

ANEWG (enhancement factor/ multiplier for the rate factor in the flow law)	1.25*3.5	3.5	0.5*3.5
ASL (basal sliding parameter) [N ⁻³ year ⁻¹ m ⁸]	1.25*1.0E-10	1.0E-10	0.5*1.0E-10
SIGMA (standard deviation melt model) [°C]	4.0	4.5	5.0
DDFS (positive-degree-day factor for snow melting) [m/yr/PDD]	0.75*0.003/0.91	0.003/0.91	1.25*0.003/0.91
DDFI (positive-degree-day factor for ice melting) [m/yr/PDD]	0.75*0.008/0.91	0.008/0.91	1.25*0.008/0.91

Table 8 : Parameter selection for three versions of AGISM along the melting axis.

Surface melting and runoff in AGISM are linked to surface temperature through the positive degree-day factors and the standard deviation ‘SIGMA’ of temperature variations around the monthly mean in the degree-day model (Janssens and Huybrechts, 2000). In GISM these parameters also influence the shape of the present-day ice sheet as surface runoff is an important ingredient of today’s mass balance. The melting strength controls mainly the area of the ice sheet but not its central thickness. To compensate for the associated volume change in the reference state, it is therefore necessary to make adjustments for the ice stiffness and the ability to slide by making concomitant changes in the flow enhancement factor and the basal sliding parameter. The latter parameters mainly control the height to width ratio, and thus ice thickness, but hardly affect surface area. It is not possible to find a parameter set that satisfies present-day constraints on both ice thickness and surface area when the melting strength is modified. For the LOVECLIM sensitivity runs, the parameter sets were chosen in order to obtain the same Greenland ice volume for the present-day. Likewise, the smaller ice sheet corresponding to the higher melting parameters also has the highest central ice thickness. The effect of the parameter choices for the three GISM runs is demonstrated in Figure 18.

The complication of present-day reference state is absent from AISM as surface runoff is negligible under the current climate. Instead, code and parameter modifications that involve basal melting below ice shelves were chosen to only influence changes with respect to the present-day reference run. This enables to use the same initial startup files for all three sensitivity versions of AISM. The basal melting rate below the ice shelves arguably constitutes the most important environmental forcing for the Antarctic ice sheet in case of moderate warming. However, its sensitivity to oceanic conditions is subject to very large uncertainties, as

is its spatial distribution below the respective ice shelves (e.g. Rignot and Jacobs, 2002). Therefore, our 3 runs vary from a case with constant basal melting ('low') to a case in which the oceanic heat input is assumed to be concentrated near to the grounding line after tripling the total amount ('high'), at which place it matters most for the position of the grounding line.

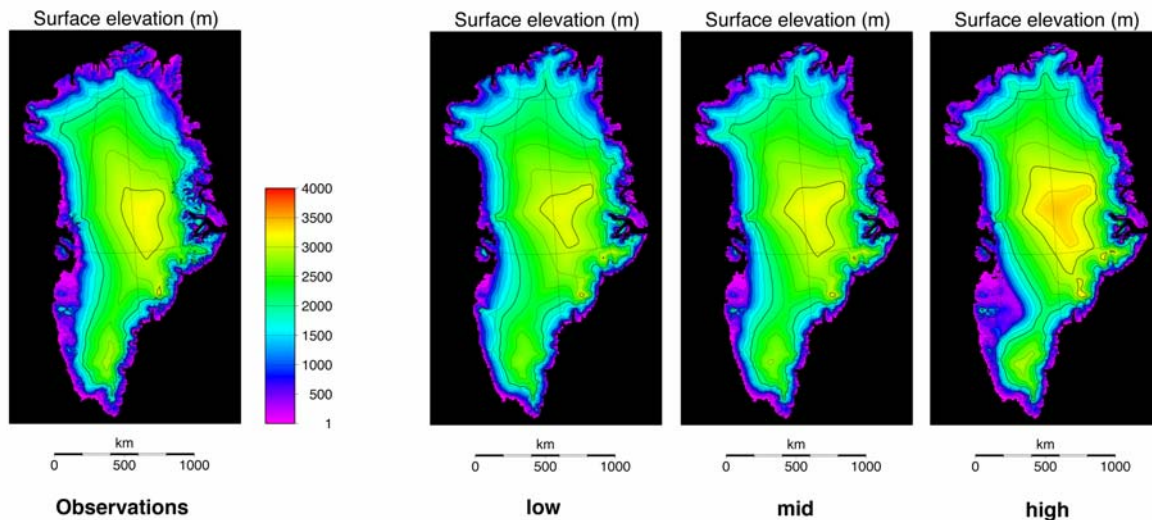


Figure 18: Modeled present-day geometries of the Greenland ice sheet corresponding to the 3 parameter sets chosen for the ASTER sensitivity runs. These all have the same ice volume at the present time. The picture at the left shows the observed surface elevation for comparison.

To demonstrate the influence of the 3 parameter sets on the behavior of AGISM, schematic offline experiments were performed under prescribed forcings, which mimic $4xCO_2$ conditions from earlier runs with LOVECLIM for a duration of 3000 years (Driesschaert et al., 2007). The main outcome of those experiments are summarized in Figure 19, Figure 20 and Figure 21 and set the stage for the forthcoming parameter variation runs over the Holocene and into the next few millennia.

For warming attaining $10^\circ C$ over Greenland, the ice sheet is found to entirely waste away over a period of between 2000 and 3000 years, in accordance with previous results. The melting is entirely driven by surface runoff of up to 10 times larger than the current amount peaking at about 0.08 Sv between 800 and 1200 years after the warming started. The total sea level rise is near to 8 m with maximum rates of between 40 cm per century (low sensitivity) and 65 cm per century (high sensitivity).

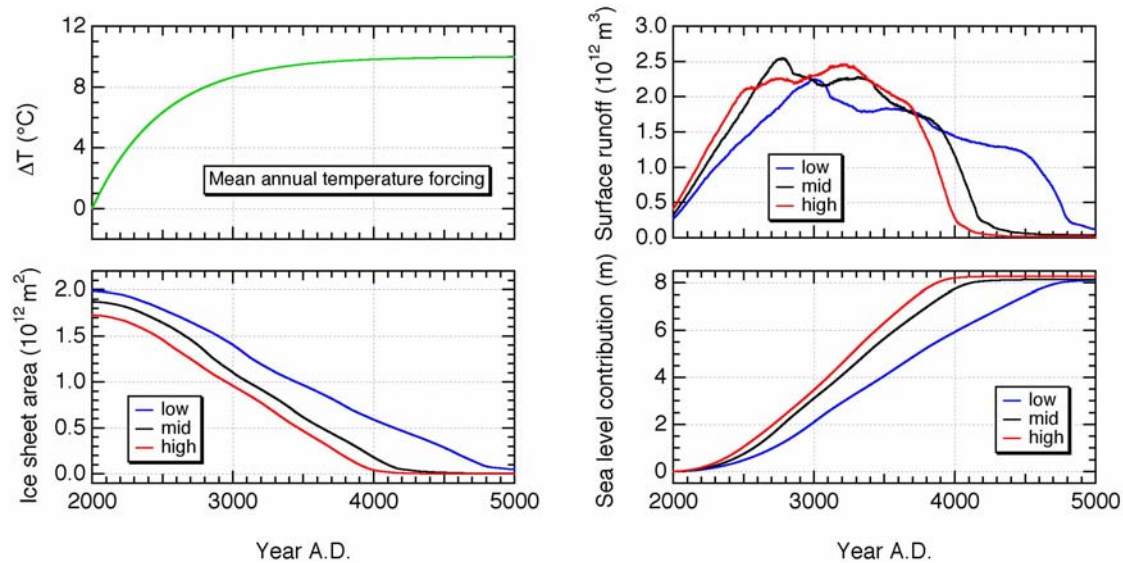


Figure 19 : Evolution of several large scale variables of the Greenland ice sheet in the 3-parameter sensitivity runs over the next 3 millennia.

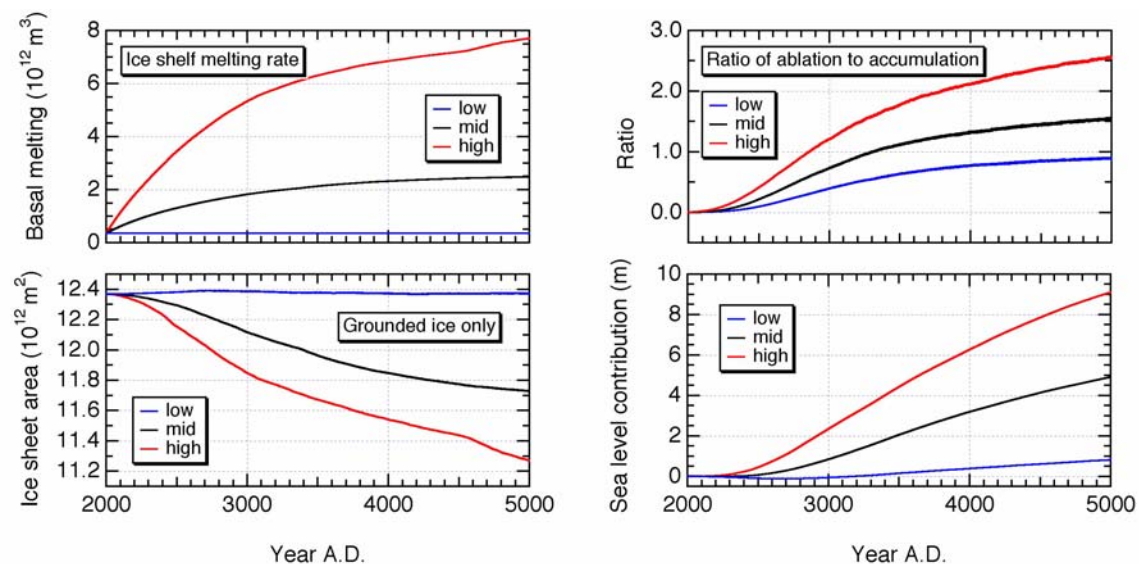


Figure 20 : Evolution of several large scale variables of the Antarctic ice sheet for the 3-parameter sensitivity runs over the next 3 millennia.

Under similar $4xCO_2$ conditions over Antarctica, the ice sheet retreat is first controlled by increased basal melting rates up to an average of 3 m/year in the high sensitivity experiment. Eventually, surface runoff takes over as the main wastage mechanism. After about 800 years of sustained warming in the high sensitivity experiment, a negative surface mass balance causes continued ice sheet retreat, which is further strengthened by the elevation/mass balance feedback. In that case, the West Antarctic ice sheet disintegrates entirely and the East Antarctic ice sheet starts to retreat on land after 3 millennia causing a total sea level rise in excess of 9 m. A stable evolution towards a new steady state under a $4xCO_2$ scenario seems only possible for the low sensitivity parameter set.

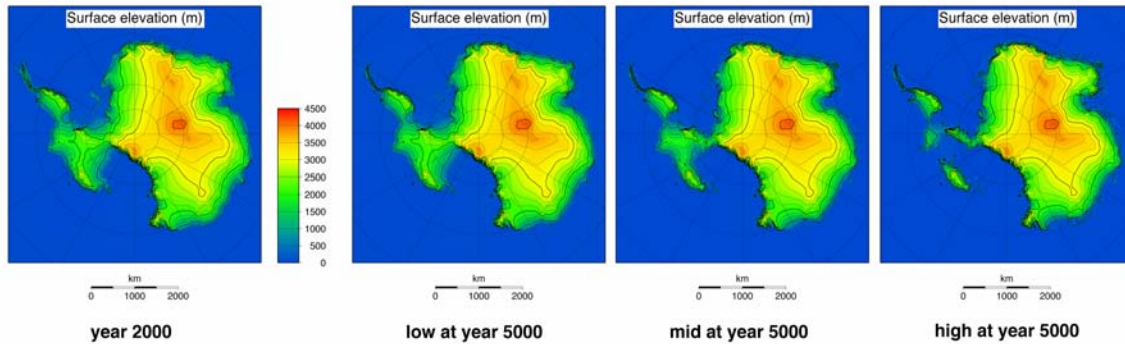


Figure 21 : Antarctic ice sheet geometries after 3000 years of 4xCO₂ conditions under the low, mid, and high parameter sets. For comparison at the left is the initial condition at the year 2000.

4. EXPERIMENTS

This section is devoted to some experiments performed with the improved version of LOVECLIM, taking advantage of the selected parameter sets, which give a range of climate responses. These experiments deal with the climate of the last millennium (section 4.2), the future sea ice extent (section 4.1) and the fate of the Greenland ice sheet under increased atmospheric CO₂ concentration (section 4.3).

4.1. The Late Holocene as a constraint for the future

In order to make a first realistic test of the method, we have performed quasi-equilibrium simulations over the early Holocene for 5 parameter sets (Experiments E11, E21, E31, E41, E51). We have then compared the results of those simulations with the ones obtained for the 21st century, using scenario SRES B1. We find a surprisingly strong relationship between the Arctic summer sea ice extent simulated for the two periods (Figure 22). In particular, the summer ice extent averaged over the period 2040-2060 is very close to 1.5 times the one simulated for 8kyr BP, for all the model simulations. This strong relationship between the simulated decrease in the summer ice extent in the future and for 8 kyr BP is obtained for a wide range of model responses despite the very different forcings during the two periods (Goosse et al., 2007). Indeed, the forcing is slowly varying for the early Holocene and has a very strong seasonal cycle. By contrast, the forcing is changing rapidly over the 20th and 21st centuries, the climate system being in a clearly transient state, and the forcing is more widely distributed for the different seasons. Information about the state of the climate system during the early Holocene would thus help us to estimate the strength of those feedbacks and thus to reduce our uncertainties on future changes. Information on the observed ice extent during the early Holocene is quite fragmentary. In the framework of the International Polar Year, new oceanic cores will be collected in the Arctic, providing new information on the summer ice extent during

the early Holocene (<http://classic.ipy.org/development/eoi/details.php?id=786>). Such observations and similar ones, in particular north of the Siberian shelves, would provide strong constraints on model behavior, complementary to the ones obtained from recent observations. This will then allow to select the parameter sets that are the most realistic and to reduce our uncertainties on the future decline of the ice cover. This is a very encouraging result for the second phase of ASTER where precisely we will use information on past change to constrain the projection.

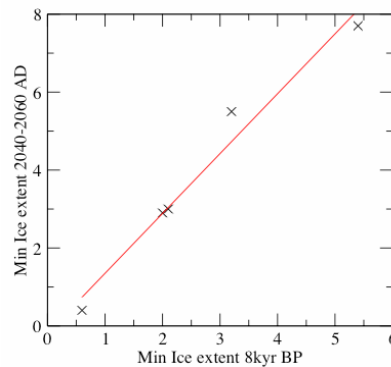


Figure 22 : Link between the Arctic summer sea ice extent (in 10^6 km^2) for the early Holocene and the period 2040-2060 A.D.. Simulations corresponding to different parameter sets (E11, E21, E31, E41, E51) are represented by a cross. The red line is a regression line for those five points.

4.2. Last millennium

The LOVECLIM model (without AGISM) has been used to simulate the climate of the last millennium with the different selected 'climate' parameter sets (i.e. experiments xx22). The purpose of these simulations was twofold. We intend to assess first the role of the carbon cycle on the climate, and second, the ability of the different selected parameter sets to drive the model within the range of the observed climate. The high frequency variability of the forcings is taken into account. For each set of parameters, LOVECLIM is driven by the natural evolution of insolation, solar irradiance and stratospheric aerosol concentrations due to volcanic activity as well as by changes caused by human activities such as deforestation, CO_2 emissions or concentration changes, changes in concentrations of greenhouse gases other than CO_2 (including ozone) and in sulphate aerosol load. For each of these forcings, a standard reconstruction has been employed (Figure 23).

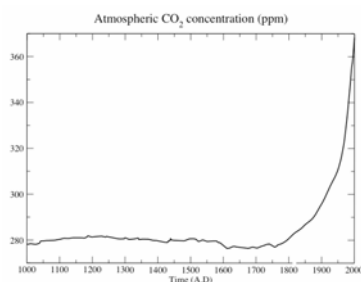


Figure 23 : Atmospheric CO₂ reconstruction used in the simulations.

Five transient experiments were conducted for each parameter set (see also Table 9). Each experiment started at 500 A.D. from an equilibrium simulation with constant forcing for that time (insolation and greenhouse gases) and went on until 2000 A.D. A first transient simulation (CONC) is forced with reconstructed atmospheric CO₂ concentration. A control simulation (CCTL), with constant greenhouse gases and insolation is also performed in order to be able to quantify any drift and to have an order of magnitude of the internal variability. In the next two simulations, the emissions of carbon were taken into account, the model computing the corresponding atmospheric CO₂ concentration. First (EMIS), the emissions due to both land use changes and fossil fuel burning were provided. Second (EFOR), only the emission of the fossil fuel burning were provided in addition to the vegetation change related to deforestation. Finally, a control simulation (ECTL) with prognostic CO₂ was performed; the forcings (insolation, greenhouse gases other than CO₂) were kept constant at their values as in 1000 A.D., no land-use scheme and no carbon emissions are considered.

Acronym	CO ₂	Insolation	GHG [‡]	Volcanism	Land-use [§]	Emissions
CONC	C	Yes	Yes	Yes	Yes	No
CCTL	500 A.D.	500 A.D.	500 A.D.	500 A.D.	No	No
EMIS	P	Yes	Yes	Yes	No	FF & LU
EFOR	P	Yes	Yes	Yes	Yes	FF
ECTL	P	500 A.D.	500 A.D.	500 A.D.	No	No

‡ All greenhouse gases except CO₂

§ Trees are replaced with grassland in accordance with Ramankutty and Foley 1700--1992 scenario (Ramankutty and Foley, 1999).

Table 9: This table gives an overview of the setup for the last millennium experiments. The experiment acronym is given in column 1. Letter *C* in column two means that atmospheric CO₂ is constrained to follow the scenario from Figure 23, while letter *P* indicates that atmospheric CO₂ is prognostic. Carbon dioxide emissions (column seven) may be restricted to fossil fuel (FF) or may include both fossil fuel and land-use change emissions (FF & LU). For control experiments, the forcings are either absent or maintained constant at their values as in 500 A.D. (CCTL and ECTL).

The simulated changes in surface temperature were first analyzed and compared to values derived from proxy records (Jansen et al., 2007).

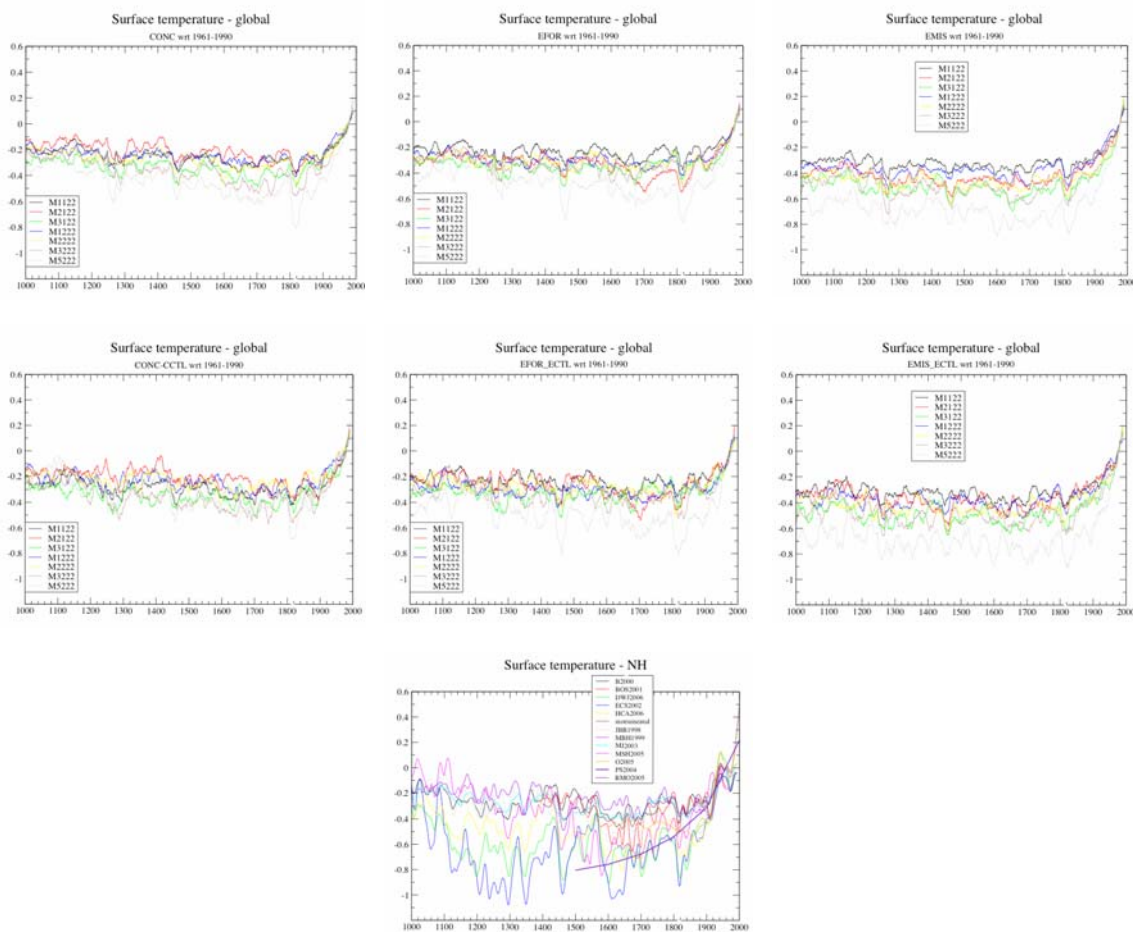


Figure 24 : (top and centre) Global annual mean surface temperature simulated with the different parameter sets and for the different hypotheses related to greenhouse gases. Raw data are displayed in the top panel and differences with the corresponding control run are depicted in the middle panel. A 21-point smoothing has been applied. (bottom) records of NH temperature variation during the last 1000 years (Jansen et al., 2007).

All temperatures represent anomalies (°C) from the 1961-1990 mean.

The global annual mean temperature simulated by the model using different parameter sets do not show striking difference (Figure 24). All the series are showing weak variability and weak trends, smaller than most of the reconstructed series. Nevertheless, slightly warmer conditions can be identified in the early part of the simulation. They are followed by a weak decrease corresponding to the Little Ice Age, which culminated around 1700 A.D. Finally, the global warming of the last century is also clearly simulated. All the simulations remain within the range of the reconstructed global temperature.

The response of the carbon cycle to the various forcings over the last millennium does not differ much among experiments (Figure 25). We choose to illustrate only two experiments; results for the remaining experiments are very close to those

illustrated in Figure 25. There is a much larger spread when considering different emission scenarios (e.g. EFOR and EMIS). The available estimates (observed atm. CO₂, ocean uptake and ocean inventory) do not easily allow to select some model versions as better than others since there are also large uncertainties associated to the land use scenario.

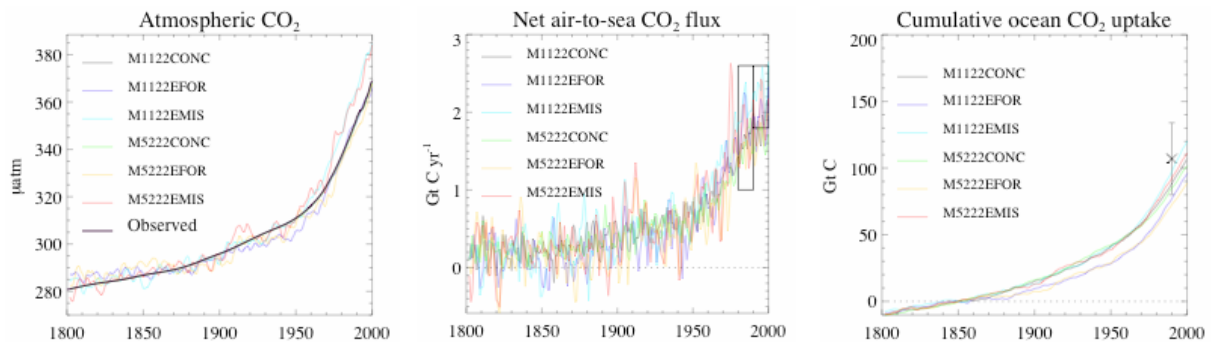


Figure 25: Evolution over the last two centuries of annual mean atmospheric CO₂ (left) and net air-sea CO₂ flux (middle). The boxes in the middle panel represent estimates for the 80's and the 90's (mean \pm standard deviation) as provided by Denman et al. (2007). The panel to the right represents the cumulative CO₂ ocean uptake relative to 1850 A.D. Reconstructed values from observations are represented by the vertical bar in 1990 A.D. (Prentice et al., 2001).

4.3. Irreversibility of a melting of the Greenland ice sheet in a warming climate

A series of preliminary experiments were performed which address the question whether the Greenland ice sheet can reform after it has melted away in a warmer climate (Goublomme and Decerf, 2007). Furthermore, it is of interest to determine the point-of-no-return during its disintegration path beyond which the melting becomes self-sustained, even if climate conditions were to return to present values (e.g. Gregory et al., 2004; Lunt et al., 2004; Toniazzo et al., 2004). We chose a CO₂ scenario that generates a strong enough warming to completely melt the Greenland ice sheet. After 3000 years, a return to glacial, preindustrial and current CO₂ levels is prescribed for the rest of the experiments (Figure 26).

We find no regrowth of the Greenland ice sheet for 380 ppm and very slow regrowth for the other two cases (Figure 27). A linear trend indicates growth times between 350 ky (200 ppm) and 1000 ky (280 ppm).

In another series of experiments (not shown), the melting process is interrupted earlier, before the Greenland ice sheet has melted away entirely, by imposing a glacial CO₂ concentration of 200 ppm. While this can stop the complete disintegration for an initially large ice sheet, there is still no regrowth. An initially small ice sheet continues to melt, but at a lower rate.

Further analyses and experiments are planned in order to determine the mechanisms controlling the long term response of the ice sheet. Because gradual cooling in response to lowering CO₂ is still ongoing after 2000 years, longer simulations are required to study regrowth, which could be possible with asynchronous coupling. One factor that influences the possible reformation may be a delayed rebound of the bedrock, which makes surface temperatures initially too warm. Furthermore, the effect of orbital parameters is not considered in the present model and the lapse rate for elevation corrections may introduce unwanted biases. Finally, the resolution of climatic input may play a crucial role in initiating or preventing the regrowth of the Greenland ice sheet.

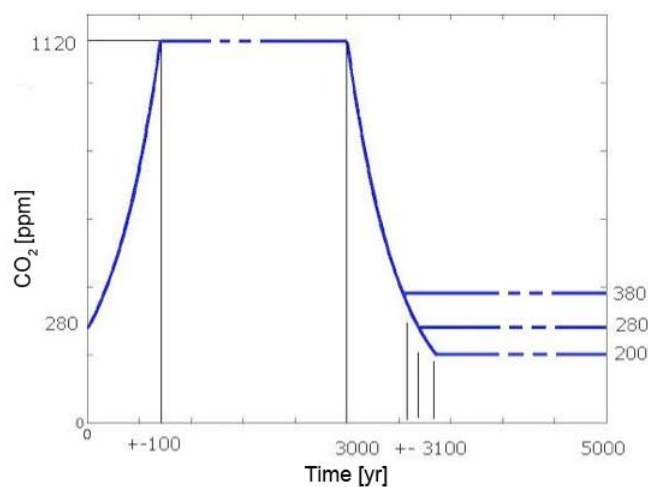


Figure 26 : CO₂ forcing scenarios to study the decay and possible regrowth of the Greenland ice sheet. The atmospheric CO₂ concentration is increased to four times the preindustrial value of 280 ppm and then held constant in order to provide a warm enough climate to completely melt the ice sheet. After 3000 years, the CO₂ concentration is reduced to 200 ppm, 280 ppm and 380 ppm corresponding to glacial, preindustrial and current CO₂ levels, respectively.

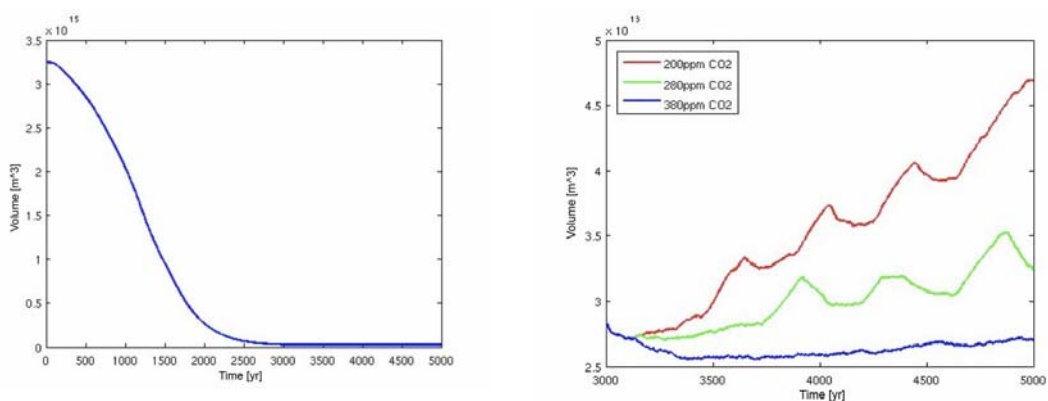


Figure 27 : Evolution of the Greenland ice volume for the three CO₂ scenarios (Figure 26). While the ice sheet does not regrow for 380 ppm, a very slow regrowth is initiated for 200 ppm and 280 ppm.

5. CONCLUSIONS AND PERSPECTIVES

The overall objective of ASTER is to provide some guidelines on the range of future climate changes, or, in other words, to try to quantify the uncertainty on projected future climate due the model itself. To reach that goal, the work during the first two years of the project was divided into two parts. First, we identified parameter sets that yield a reasonable simulation of the present-day climate, ice sheets and carbon cycle, and that lead to contrasted responses to a doubling of the atmospheric CO₂ concentration and to a freshwater hosing. Second, we simulated past climates (last millennium, Holocene) using these parameters sets. Our purpose here was to select those parameter sets that are able to simulate relatively well these past climates. Further simulations must still be performed to short-list the parameter sets that best simulate past and present climates. In the next two years, the climate of the next millennium will be simulated focusing on the stability of the North Atlantic MOC, the Greenland and Antarctic ice sheets, the biogeochemical feedbacks and the impact of all these processes on climate and sea level. Although most of the simulations must still be undergone, we already demonstrated how the summer arctic sea ice extent during the Holocene could give an insight on the future evolution of the Arctic ice pack. The possible irreversibility of a disappearance of the Greenland ice sheet in a warming climate has also been tested in a series of experiments.

REFERENCES

- Archer, D., Kheshgi, H. and Maier-Reimer, E. 1998. Dynamics of fossil fuel CO₂ neutralization by marine CaCO₃. *Global Biogeochemical Cycles*, 12, 259-276.
- Archer, D. 2003. Biological fluxes in the ocean and atmospheric CO₂. In : H. Elderfield (ed), *Treatise on Geochemistry, Volume 6, The Oceans and Marine Geochemistry*.
- Berger, W. H., Fischer, K., Lai, C. and Wu, G. 1987. Ocean Productivity and Organic Carbon Flux. Part I. Overview and Maps of Primary Production and Export Production, University of California, SCRIPPS Institution of Oceanography, SIO Ref 87-30.
- Betzer, P. R., Byrne, R. H. , Acker, J. G., Lewis, C. S. and Jolley, R. R. 1984. The oceanic carbonate system: a reassessment of biogenic controls, *Science*, 226, 1074-1077.
- Beckmann, A. and Goosse, H. 2003. A parameterization of ice shelf-ocean interaction for climate models. *Ocean modelling*, 5, 157-170.
- Braconnot, P., Loutre, M. F., Dong, B., Joussaume, S. and Valdes, P. 2002. How the simulated change in monsoon at 6 ka BP is related to the simulation of the modern climate: results from the Paleoclimate Modeling Intercomparison Project. *Climate Dynamics*, 19, 107-121.
- Broecker, W., Clark, E., McCorkle, D., Peng, T., Hajdas, I. and Bonani, G. 1999. Evidence for a reduction in the carbonate ion content of the deep sea during the course of the Holocene. *Paleoceanography*, 14, 744-752.
- Broecker, W. S. and Clark, E. 2002. Holocene atmospheric CO₂ increase as viewed from the seafloor. *Global Biogeochemical Cycles*, 17, 1052 (doi:10.1029/2002GB001985).
- Brovkin, V., Ganopolski, A. and Svirezhev, Y. 1997. A continuous climate-vegetation classification for use in climate-biosphere studies. *Ecological Modelling*, 101, 251-261.
- Brovkin, V., Bendtsen, J., Claussen, M., Ganopolski, A. , Kubatzki, C., Petoukhov, V. and Andreev, A. 2002. Carbon cycle, vegetation, and climate dynamics in the Holocene: Experiments with the CLIMBER-2 model. *Global Biogeochemical Cycles*, 16, 1139 (doi: 10.1029/2001GB001662).
- Bryan, K. and Lewis, L.J. 1979. A water mass model of the world ocean. *J. Geophys. Res.*, 84 (C5), 2503-2517.

- Bidle, K. D., Manganalli, M. and Azam, F. 2002. Regulation of oceanic silicon and carbon preservation by temperature control on bacteria, *S*, 298, 1980-1984.
- Boyer, T.P., Antonov, J.I. , Garcia, H.E., Johnson, D.R., Locarnini, R.A., Mishonov, A.V., Pitcher, M.T., Baranova, O.K., Smolyar, I.V. 2006. World Ocean Database 2005. In : S. Levitus (Ed.), NOAA Atlas NESDIS 60, U.S. Government Printing Office, Washington, D.C., 190 pp., DVDs.
- Chou C. and Neelin, J.D. 1996. Linearization of a long-wave radiation scheme for intermediate tropical atmospheric model. *J. Geophys. Res.* ,101 (D10), 15129-15145.
- Clarke, G. K. C., Leverington, D. W., Teller, J. T. and Dyke, A. S. 2004. Paleohydraulics of the last outburst flood from glacial Lake Agassiz and the 8200 BP cold event. *Quat. Sc. Rev.*, 23, 389-407.
- Covey, C., AchutaRao, K. M., Lambert, S. J. and Taylor, K. E. 2000. Intercomparison of present and future climates simulated by coupled ocean-Atmosphere GCMs. PCMDI Report 66, Program for Climate Diagnosis and Intercomparison, Lawrence Livermore National Laboratory, University of California, Livermore, CA
- Cox, P., Betts, R., Jones, C., Spall, S. and Totterdell, I. 2000. Acceleration of global warming due to carbon-cycle feedbacks in a coupled climate model. *Nature*, 408, 184-187.
- Denman, K.L., Brasseur, G., Chidthaisong, A., Ciais, P., Cox, P.M., Dickinson, R.E., Hauglustaine, D., Heinze, C., Holland, E., Jacob, D., Lohmann, U., Ramachandran, S., da Silva Dias, P.L., Wofsy, S.C. and Zhang, X. 2007. Couplings Between Changes in the Climate System and Biogeochemistry. In: Climate Change 2007: The Physical Science Basis. Contribution of Working Group I to the Fourth Assessment Report of the Intergovernmental Panel on Climate Change [Solomon, S., D. Qin, M. Manning, Z. Chen, M. Marquis, K.B. Averyt, M. Tignor and H.L. Miller (eds.)]. Cambridge University Press, Cambridge, United Kingdom and New York, NY, USA.
- Driesschaert, E., Fichet, T., Goosse, H., Huybrechts, P., Janssens, I., Mouchet, A., Munhoven, G., Brovkin, V. and Weber, S.L. 2007. Modeling the influence of Greenland ice sheet melting on the meridional overturning circulation during the next millennia. *Geophysical Research Letters*, L10707. doi:10.1029/2007GL029516.
- Dutay, J.-C., Jean-Baptiste, P., Campin, J.-M., Ishida, A., Maier-Reimer, E., Matear, R.J., Mouchet, A., Totterdell, I.J., Yamanaka, Y. , Rodgers, K., Madec, G., Orr, J.C. 2004. Evaluation of OCMIP-2 ocean models' deep circulation with mantle helium-3. *J. Mar. Systems*, 48, 15-36, doi:10.1016/j.jmarsys.2003.05.010.

- ETOPO5. 1988. Data Announcement 88-MGG-02, Digital relief of the Surface of the Earth. NOAA, National Geophysical Data Center, Boulder, Colorado, <http://www.ngdc.noaa.gov/mgg/global/etopo5.HTML>
- Fichefet, T., Poncin, C., Goosse, H., Huybrechts, P., Janssens, I. and Treut, H. L. 2003. Implications of changes in freshwater flux from the Greenland ice sheet for the climate of the 21st century. *Geophysical Research Letters*, 30, 1911 (doi:10.1029/2003GL017826).
- Fichefet, T., Driesschaert, E., Goosse, H., Huybrechts, P., Janssens, I., Mouchet, A. and Munhoven, G. 2007. Modelling the climate and sea level during the third millennium (MILMO), Scientific Support Plan for a Sustainable Development Policy, Belgian Science Policy, 131 p.
- Flückiger, J., Monnin, E., Stauffer, B., Schwander, J., Stocker, T., Chappellaz, J., Raynaud, D. and Barnola, J.-M. 2002. High-resolution Holocene N₂O ice core record and its relationship with CH₄ and CO₂. *Global Biogeochemical Cycles*, 16, Art. No. 1010.
- Friedlingstein, P., Bopp, L., Ciais, P., Dufresne, J., Faihead, L., LeTreut, H., Monfray, P. and Orr, J. 2001. Positive feedback between future climate change and the carbon cycle. *Geophys. Res. Lett.*, 28, 1543-1546.
- Friedlingstein, P., Cox, P., Betts, R., Bopp, L., von Bloh, W., Brovkin, V., Cadule, P., Doney, S., Eby, M., Fung, I., Bala, G., John, J., Jones, C., Joos, F., Kato, T., Kawamiya, M., Knorr, W., Lindsay, K., Matthews, H. D., Raddatz, T., Rayner, P., Reick, C., Roeckner, E., Schnitzler, K.-G., Schnur, R., Strassmann, K., Weaver, A. J., Yoshikawa, C. and Zeng, N. 2006. Climate–Carbon Cycle Feedback Analysis: Results from the C4MIP Model Intercomparison. *J. Clim.*, 19, 3337-3353.
- Fujii, M. and Chai, F. 2005. Effects of biogenic silica dissolution on silicon cycling and export production, *Geophysical Research Letters*, 32, L05617, doi:10.1029/2004GL022054.
- Goublomme, V. and Decerf, B. 2007. La fonte de l'inlandsis du Groenland au cours des prochains millénaires est-elle irréversible?. MSc thesis UCL.
- Goosse H., Deleersnijder, E., Fichefet, T. and England, M.H. 1999. Sensitivity of a global coupled ocean-sea ice model to the parameterization of vertical mixing. *Journal of Geophysical Research*, 104(C6), 13681-13695.
- Goosse, H., Selten, F. M., Haarsma, R. J. and Opsteegh, J. D. 2001. Decadal variability in high northern latitudes as simulated by an intermediate-complexity climate model. *Ann. of Glaciol.*, 33, 525-532.

- Goosse H., Driesschaert, E., Fichet, T. and Loutre, M.F. 2007. Information on the early Holocene climate constrains the summer sea ice projections for the 21st century. *Clim. Past.*, Vol.3, pp. 683-692, SRef-ID: 1814-9332/cp/2007-3-683.
- Gregory, J. M., Huybrechts, P. and Raper, S. C. B. 2004. Threatened loss of the Greenland ice sheet. *Nature*, 428, 616.
- Gregory, J. M., Dixon, K. W., Stouffer, R. J., Weaver, A. J., Driesschaert, E., Eby, M., Fichet, T., Hasumi, H., Hu, A., Jungclaus, J. H., Kamenkovich, I. V., Levermann, A., Montoya, M., Murakami, S., Nawrath, S., Oka, A., Sokolov, A. P. and Thorpe, R. B. 2005. A model intercomparison of changes in the Atlantic thermohaline circulation in response to increasing atmospheric CO₂ concentration. *Geophys. Res. Lett.*, 32, L12703 (doi:10.1029/2005GL023209).
- Haarsma, R.J., Selten, F.M., Opsteegh, J.D., Lenderink, G. and Liu., Q. 1996. ECBILT, a coupled atmosphere ocean sea-ice model for climate predictability studies. KNMI, De Bilt, The Netherlands, 31 pp.
- Hasselmann, K., Latif, M., Hooss, G., Azar, C., Edenhofer, O., Jaeger, C. C., Johannessen, O. M., Kemfert, C., Welp, M. and Wokaun, A. 2003. The challenge of long-term climate change. *Science*, 302, 1923-1925.
- Heinze, C. 2004. Simulating oceanic CaCO₃ export production in the greenhouse. *Geophys. Res. Lett.*, 31, L16308, doi:10.1029/2004GL020613.
- Houghton, J.T., Ding, Y., Griggs, D.J., Noguer, M., van der Linden, P.J., Dai, X., Maskell, K. and Johnson, C.A. 2001. Climate Change 2001: The Scientific Basis. Contribution of Working Group I to the Third Assessment Report of the Intergovernmental Panel on Climate Change. Cambridge University Press, 881 pp.
- Huybrechts, P., 2002. Sea-level changes at the LGM from ice-dynamic reconstructions of the Greenland and Antarctic ice sheets during the glacial cycles. *Quat. Sc. Rev.*, 21, 203-231.
- Huybrechts, P. and T'siobbel, S. 1997. A three-dimensional climate/ ice-sheet model applied to the Last Glacial Maximum. *Ann. of Glaciol.*, 25, 333-339.
- Indermühle, A., Stocker, T., Joos, F., Fischer, H., Smith, H., Wahlen, M., Deck, B., Mastroianni, D., Tschumi, J., Blunier, T., Meyer, R. and Stauffer, B. 1999. Holocene carbon-cycle dynamics based on CO₂ trapped in ice at Taylor Dome, Antarctica. *Nature*, 398, 121-126.
- Houghton, J.T., Ding, Y., Griggs, D.J., Noguer, M., van der Linden, P.J., Dai, X., Maskell, K. and Johnson, C.A. 2001. Climate Change 2001: The Scientific Basis. Contribution of Working Group I to the Third Assessment Report of the

- Intergovernmental Panel on Climate Change. Cambridge University Press, 881 pp.
- Jansen, E., Overpeck, J., Briffa, K.R., Duplessy, J.-C., Joos, F., Masson-Delmotte, V., Olago, D., Otto-Bliesner, B., Peltier, W.R., Rahmstorf, S., Ramesh, R., Raynaud, D., Rind, D., Solomina, O., Villalba, R. and Zhang, D. 2007. Palaeoclimate. In: *Climate Change 2007: The Physical Science Basis. Contribution of Working Group I to the Fourth Assessment Report of the Intergovernmental Panel on Climate Change* [Solomon, S., D. Qin, M. Manning, Z. Chen, M. Marquis, K.B. Averyt, M. Tignor and H.L. Miller (eds.)]. Cambridge University Press, Cambridge, United Kingdom and New York, NY, USA.
- Janssens, I. and Huybrechts, P. 2000. The treatment of meltwater retention in mass-balance parameterizations of the Greenland ice sheet. *Annals of Glaciology*, 31, 133-140.
- Johnson, J. and Fastook, J. L. 2002. Northern hemisphere glaciation and its sensitivity to basal melt water. *Quaternary International*, 95-96.
- Jones, C., Gregory, J., Thorpe, R., Cox, P., Murphy, J., Sexton, D. and Valdes, P. 2005. Systematic optimisation and climate simulation of FAMOUS, a fast version of HadCM3. *Clim. Dyn.*, 25 (2-3), 189-204.
- Joos, F., Meyer, R., Bruno, M. and Leuenberger, M. 1999. The variability in the carbon sinks as reconstructed for the last 1000 years. *Geophys. Res. Lett.*, 26, 1437-1440.
- Joos, F., Gerber, S., Prentice, I., Otto-Bliesner, B. and Valdes, P. 2004. Transient simulations of Holocene atmospheric carbon dioxide and terrestrial carbon since the Last Glacial Maximum. *Global Biogeochemical Cycles*, 18, Art. No. GB2002.
- Key, R.M., Kozyr, A., Sabine, C.L., Lee, K., Wanninkhof, R., Bullister, J., Feely, R.A., Millero, F., Mordy, C., Peng, T.-H. 2004. A global ocean carbon climatology: Results from GLODAP. *Global Biogeochemical Cycles*, 18, GB4031.
- Klaas, C. and Archer, D. 2002. Association of sinking organic matter with various types of mineral ballast in the deep sea: Implications for the rain ratio. *Global Biogeochemical Cycles*, 16, 1116, doi:10.1029/2001GB001765.
- Kitoh, A. and Murakami, S. 2002. Tropical Pacific Climate at the mid-Holocene and the Last Glacial Maximum simulated by a coupled ocean-atmosphere general circulation model. *Paleoceanography*, 17, 1-13.
- Lunt, D., de Noblet-Ducoudré, N. and Charbit, S. 2004. Effects of a melted Greenland ice sheet on climate, vegetation, and the cryosphere. *Climate Dynamics*, 23, 679-694.

- Maier-Reimer, E., Mikolajewicz, U. and Winguth, A. 1996. Future ocean uptake of CO₂: interaction between ocean circulation and biology. *Clim.Dyn.*, 12, 711-721.
- Marchal, O., 2005: Optimal estimation of atmospheric C-14 production over the Holocene: paleoclimate implications. *Clim.Dyn.*, 24, 71-88.
- Martin, J. H., Knauer, G. A., Karl, D. M. and Broenkow, W. W. 1987. VERTEX: carbon cycling in the northeast Pacific, *Deep Sea Res.*, 34, 267-285, 1987.
- Munhoven, G. 2007. Glacial–interglacial rain ratio changes: Implications for atmospheric CO₂ and ocean–sediment interaction. *Deep-Sea Research*, 54, 722-746.
- Murphy, J. M., Sexton, D. M. H. , Barnett, D. N., Jones, G. S., Webb, M. J., Collins, M. and Stainforth, D. A. 2004. Quantification of modelling uncertainties in a large ensemble of climate change simulations. *Nature*, 430, 768-772.
- Mouchet, A. and François, L. M. 1996. Sensitivity of a global oceanic carbon cycle model to the circulation and to the fate of organic matter : preliminary results. *Phys. Chem. Earth*, 21, 511-516.
- Najjar, R. G., Jin, X., Louanchi, F., Aumont, O. , Caldeira, K., Doney, S. C., Dutay, J.-C., Follows, M., Gruber, N., Joos, F., Lindsay, K., Maier-Reimer, E., Matear, R. J., Matsumoto, K., Mouchet, A., Orr, J. C., Plattner, G.-K., Sarmiento, J. L., Schlitzer, R., Weirig, M. F., Yamanaka and, Y., and Yool, A. 2007. Impact of circulation on export production, dissolved organic matter and dissolved oxygen in the ocean: Results from OCMIP-2. *Global Biogeochem. Cycles*, 21 (3), article GB3007.
- Nelson, D. M., Tréguer, P., Brzezinski, M. A., Leynaert and, A. and Quéguiner, B. 1995. Production and dissolution of biogenic silica in the ocean: revised global estimates, comparison with regional data and relationship to biogenic sedimentation, *Global Biogeochem. Cycles*, 9, 359-372.
- NOCES HowTo 2003. NOCES Interannual HOWTO document. <http://www.ipsl.jussieu/projets/NOCES>.
- Opsteegh, J. D., Haarma, R. J., Selten, F. M. and Kattenberg, A. 1998. EC-BILT: a dynamic alternative to mixed boundary conditions in ocean models. *Tellus Series a-Dynamic Meteorology and Oceanography*, 50, 348-367.
- Orr, J. C., Fabry, V. J, Aumont, O., Bopp, L., Doney, S. C., Feely, R. M., Gnanadesikan, A., Gruber, N., Ishida, A., Joos, F., Key, R. M., Lindsay, K., Maier-Reimer, E., Matear, R., Monfray, P., Mouchet, A., Najjar, R. G., Plattner, G.-K., Rodgers, K. B., Sabine, C. L., Sarmiento, J. L., Schlitzer, R., Slater, R. D., Totterdell, I., Weirig, M.-F., Yamanaka, Y. and Yool, A. 2005. Anthropogenic

- ocean acidification over the 21st century and its impact on marine calcifying organisms. *Nature*, 437 (7059), 681-686.
- Parizek, B. R. and Alley, R. B. 2004. Implications of increased Greenland surface melt under global-warming scenarios: ice-sheet simulations. *Quat. Sc. Rev.*, 23, 1013-1027.
- Pitman, A.J., and Stouffer, R. J. 2006. Abrupt change in climate and climate models. *Hydrology and Earth System Sciences*, 10, 903-912.
- Prentice, I.C., Farquhar, G. D., Fasham, M., Goulden, M., Heimann, M., Jamarillo, V., Keshgi, H., Le Quéré, C., Scholes, R., Wallace, D. 2001. The carbon cycle and atmospheric carbon dioxide. In : *Climate Change 2001. The scientific basis*. J. T. Houghton, Y. Ding, D. J. Griggs, M. Noguer, P.J. van der Linden, X. Dai, K. Maskell and C. A. Johnson (eds), Cambridge University Press, Cambridge, UK and New York, U.S.A.
- Ramankutty, N. and Foley, J. 1999. Estimating historical changes in global land cover: Croplands from 1700 to 1992, *Global Biogeochemical Cycles*, 13, 997-1027.
- Raper, S. and Braithwaite, R. 2005. The potential for sea level rise: New estimates from glacier and ice cap area and volume distributions. *Geophys. Res. Lett.*, 32, Art. No. L05502.
- Raper, S. C. B. and Braithwaite, R. J. 2006. Low sea level rise projections from mountain glaciers and icecaps under global warming. *Nature*, 439, 311-313.
- Reich, P. B., Hobbie, S. E., Lee, T., Da. S. Ellsworth, West, J. B., Tilman, D., Knops, J. M. H., Naeem, S. and Trost, J. 2006. Nitrogen limitation constrains sustainability of ecosystem response to CO₂. *Nature*, 440, 922-925, doi:10.1038/nature04486.
- Renssen, H., Goosse, H., Fichefet, T. and Campin, J. M. 2001. The 8.2 kyr BP event simulated by a global atmosphere-sea-ice-ocean model. *Geophys. Res. Lett.*, 28, 1567-1570.
- Rignot, E. J. and Jacobs, S. J. 2002. Rapid bottom melting widespread near Antarctic ice sheet grounding lines. *Science*, 296, 2020-2023.
- Sarmiento, J.L., Hughes, T. M., Stouffer, R. J. and Manabe, S. 1998. Simulated response of the ocean carbon cycle to anthropogenic climate warming, *Nature*, 393, 245-249.
- Schaeffer M., Selten, F., van Dorland, R. 1998. Linking Image and ECBILT. National Institute for public health and the environment (RIVM), Bilthoven, The Netherlands, Report no 4815008008.

- Schmidt, G. A. and LeGrande, A. N. 2005. The Goldilocks abrupt climate change event. *Quat. Sc. Rev.*, 24, 1109-1110.
- Schmittner, A., 2005. Decline of the marine ecosystem caused by a reduction in the Atlantic overturning circulation. *Nature*, 434, 628-633.
- Shine, K.P. and Henderson-Sellers, A. 1985. The sensitivity of a thermodynamic sea ice model to changes in surface albedo parameterization. *J. Geophys. Res.* , 90(D1), 2243-2250
- Stainforth, D. A., Aina, T., Christensen, C., Collins, M., Faull, N., Frame, D. J., Kettleborough, J. A., Knight, S., Martin, A., Murphy, J. M., Piani, C., Sexton, D., Smith, L. A., Spicer, R. A, Thorpe, A. J. and Allen, M. R. 2005. Uncertainty in predictions of the climate response to rising levels of greenhouse gases. *Nature*, 433, 403-406.
- Suess, E. 1980. Particulate organic carbon flux in the ocean - surface productivity and oxygen utilization, *Nature*, 288, 260-263.
- Takahashi, T., Sutherland, S., Sweeney, C., Poisson, A., Metzl, N., Tilbrook, B., Bates, N., Wanninkhof, R., Feely, R., Sabine, C., Olafsson, J. and Nojiri, Y. 2002. Global sea-air CO₂ flux based on climatological surface ocean pCO₂ and seasonal biological and temperature effects. *Deep-Sea Research*, 49, 1601-1622.
- Tarasov, L. and Peltier, W. R. 2005. Arctic freshwater forcing of the Younger Dryas cold reversal. *Nature*, 435, 662-665.
- Taylor, K. E. 2001. Summarizing multiple aspects of model performance in a single diagram, *Journal of Geophysical Research*, 106, 7183-7192.
- Thompson, S.T., Govindasamy, B., Mirin, A., Caldeira, K., Delire, C., Milovich, J., Wickett, M. and Erickson, D. 2004. Quantifying the effects of CO₂-fertilized vegetation on future global climate and carbon dynamics. *Geophys. Res. Letters*, 31, L23211 (doi:10.1029/2004GL021239).
- Toniazzo, T., Gregory, J. M. and Huybrechts, P. 2004. Climatic impact of a Greenland deglaciation and its possible irreversibility. *Journal of Climate*, 17 (1), 21-33.
- Tsunogai, S. , and Noriki, S. 1991. Particulate fluxes of carbonate and organic carbon in the ocean. Is the marine biological activity working as a sink of the atmospheric carbon? *Tellus*, 43, 256-266.
- Vaughan, D. G. and Spouge, J. 2002. Risk estimation of collapse of the West Antarctic ice sheet. *Climatic Change*, 52, 65-91.

- Verdin, E. 2006. Variabilité interannuelle des échanges de CO₂ entre l'atmosphère et l'océan. Undergraduate thesis. University of Liège.
- Zondervan, I., Zeebe, R., Rost, B. and Riebesell, U. 2001. Decreasing marine biogenic calcification: A negative feedback on rising atmospheric pCO₂. *Global Biogeochem. Cycles*, 15, 507-516.
- Zweck, C. and Huybrechts, P. 2005. Northern hemisphere ice sheet modeling of the last glacial cycle and glaciological sensitivity. *J. Geophys. Res.*, 110, D07103 (doi:10.1029/2004JD005489).
- Zweck, C. and Huybrechts, P. 2003. Modeling the marine extent of northern hemisphere ice sheets during the last glacial cycle. *Annals of Glaciology*, 37, 173-180.